Considering buried depth in the moving finite line source model for vertical borehole heat exchanges – a new solution

by

Yunting Guo

A thesis submitted in partial fulfillment of the requirements for the degree of

Master of Science

in

Mining Engineering

Department of Civil and Environmental Engineering
University of Alberta

Abstract

The current available *g*-functions obtained from the moving finite line source (MFLS) model for design and simulation of vertical borehole heat exchangers (BHEs) neglects the effects of buried depth, i.e. the vertical distance between the ground surface and the BHEs. This study proposed a new analytical solution of the MFLS model in a single integral form that extends the validity of the MFLS model by taking the effects of buried depth into consideration. Furthermore, the spatial superposition technique was employed to computing new *g*-functions using the new proposed analytical solution for multiple borehole field. A customized MATLAB code was deployed to compute the new proposed solution and the new *g*-functions. The correctness of them was numerically verified with an equivalent three-dimensional (3D) finite-element (FE) model developed in COMSOL Multiphysics software. A sensitivity study was carried out to investigate the influence of the buried depth. Results reveal that the new proposed solution must be used over the standard MFLS model to consider the combined effects of buried depth and groundwater flow when calculating the temperature variation of the Peclet number (Pe) < 22. The findings also indicate that the effects of buried depth increase as the borehole length decreases, and the effect of buried depth is more significant in a borehole field containing multiple boreholes due to the accumulation effects of the buried borehole. Neglecting buried depth could result in an under-estimation of the temperature variation by more than 8%. Therefore, the buried depth becomes an important parameter in the design of BHEs.

Preface

This thesis is an original work by Yunting Guo. Chapter 2 and Appendix A of this thesis has been published as Y. Guo, J. Komar, W.V. Liu, M. Sepehri, and Y. Pourrahimian, "Considering Groundwater advection on the Design of Borehole Heat Exchanger—A Review of Analytical Solutions," GeoEdmonton 2018. Chapters 3 and 4 of this thesis has been submitted for peer review as Y. Guo, X. Hu, J. Banks, and W.V. Liu, "Considering buried depth in the moving finite line source model for vertical borehole heat exchangers—a new solution," Energy and Buildings.

Acknowledgement

First and foremost, I would like to express my sincere gratitude to my supervisor, Dr. Wei Victor Liu, for his inspiring guidance and encouragement through my work and for the priceless influence he has made in my academic life.

I am thankful to all the colleagues in my research group, who have helped me through my studies, who have inspired me, and with whom I have established friendship that I cherish in my life. Special thanks go to Alex Hu, Linping Wu, Guangping Huang and Shaosen Ma.

Nevertheless, I wish to give thanks to all my friends who enriched my graduate life.

Finally, I am extremely grateful for the support and endless love I received from my parents. I would have not been able to accomplish this without her support and love.

Also, my greatest grateful words are dedicated to my love, Jingwen Wang, for always being there to help and support me, to care and encourage me, and for always being patient with me.

Contents

List of Figures

List of Tables

Nomenclature

c	specific heat capacity	[$Jkg^{-1}K^{-1}$]
D	buried depth	[m]
d	$= D/H$	
$E_1(X)$	exponential integral function	
$erf(X)$	error function	
$erfc(X)$	complementary error function	
Fo	Fourier number	
$g(x_1, x_2, \cdots)$	g-function	
H	borehole length	[m]
I_0	modified zero order Bessel function of the first kind	
k	thermal conductivity	[$Wm^{-1}K^{-1}$]
N	Number of observations	
Pe	Peclet number	
q_l	heat flow rate per unit length of the borehole	[Wm^{-1}]
r, r'	radial distance to the source	[m]
r_b	radius of the borehole [m]	
R_b	$= r_b/H$	
s	$= \frac{1}{\sqrt{4\alpha(t-t')}}$	
t, t'	time	[s]

T	temperature	[°C]
T_b	borehole wall temperature	[°C]
T_0	undisturbed ground temperature	[°C]
ΔT	temperature variation	[°C]
U	$= \frac{u_d \rho_w c_w}{\rho c}$	[ms^{-1}]
u_d	groundwater velocity	[ms^{-1}]
X, Y	arguments of functions	
x, y, z, z'	coordinates	[m]

Greek symbols

α	thermal diffusivity	[m^{2}s^{-1}]
β	$= \frac{r}{\sqrt{4\alpha(t-t')}}$	
γ, γ'	$= \sqrt{r^2 + (z \pm z')^2}$	
ϕ	$= r^2 / (4\alpha(t-t'))$	
φ	cylindrical coordinate	
ξ	$= \beta^2$	
ρ	density	[kgm^{-3}]
Θ	$= 2\pi k \Delta T / q_l$	

Subscripts

A	analytical model
C	3D-FE COMSOL model

b	borehole
l	line source
w	water

Superscripts

$\bar{}$	$= \frac{1}{H}\int_0^H \cdots \, dz'$	integral mean

List of Abbreviations

BHE	Borehole heat exchanger
FE	Finite element
FLS	Finite line source
GSHP	Ground source heat pump
ILS	Infinite line source
LTE	Local thermal equilibrium
MAE	Mean absolute error
MFLS	Moving finite line source
MILS	Moving infinite line source
RMSD	Root mean square deviation

1. Introduction

1.1. Research background

In Canada, mining activities usually need a huge amount of energy from burning fossil fuels for heating purpose due to the long last cold winter [1]. As an example, in underground mine operations, fresh air has to be pre-heated to a sufficient temperature (1.5 °C), preventing the seeped groundwater from freezing in the ventilation shafts [2]; and the pre-heating costs millions of gallons of natural gas or propane annually [3]. To reduce the considerably fossil fuels consumption for heating, applications of ground source heat pump (GSHP) rise great attention in the mining sector [4, 5].

GSHP systems, also known as shallow geothermal or geoexchange systems, have been utilized in residential and commercial buildings to provide space heating and cooling. From 2010 to 2015, the installed capacity of GSHP systems has grown by 52%, from 33,134 MWt to 50,258 MWt, while the corresponding annual geothermal energy utilized has grown by 63%, from 200,149 TJ to 326,848 TJ [6]. The GSHP system has been receiving escalating interest due to its high energy efficiency, low electricity consumption, and the potential to reduce greenhouse gas emissions [7].

The GSHP system uses the ground as a heat source or a heat sink. The ground is a desirable thermal energy reservoir because the ground temperature remains relatively constant below a certain depth throughout the year [8]. For example, in Canada, the shallow ground temperature is commonly within a range of 6 °C to 12 °C, and this temperature is relatively constant. The constant temperature is caused by the high thermal inertia of soil and rock. Thermal inertia represents the tendency of soil and rock to resist

temperature changes; it diminishes the influence of the ground surface temperature fluctuations as the depth increases [8, 9], providing the potential for using GSHP system [10].

In general, the GSHP system has two common layouts — one that is horizontal and the one that is vertical [11]. In comparison with the horizontal layout, the vertical layout requires a relatively smaller ground area, has a more stable heat source, and provides more efficient performance [11, 12]. In a vertical GSHP system, the heat pump is normally combined with a set of borehole heat exchangers (BHEs). These BHEs are used for heat extraction from (or heat injection into) the subsurface (see Fig. 1) [13]. The most common form of BHE is a vertical closed loop system that has single U-tubes made of high-density polyethylene pipes. These pipes are installed into multiple vertical boreholes down to a depth ranging from 50 m to 150 m [14]. Boreholes are typically 0.1 m to 0.15 m in diameter [15]. The performance of the BHE is crucial to the success of the GSHP system because it determines the amount of thermal energy extraction from the ground [16]. For a successful GSHP system, the performance of BHE is required for satisfying the a project's thermal energy demand during the life cycle of the system [16].

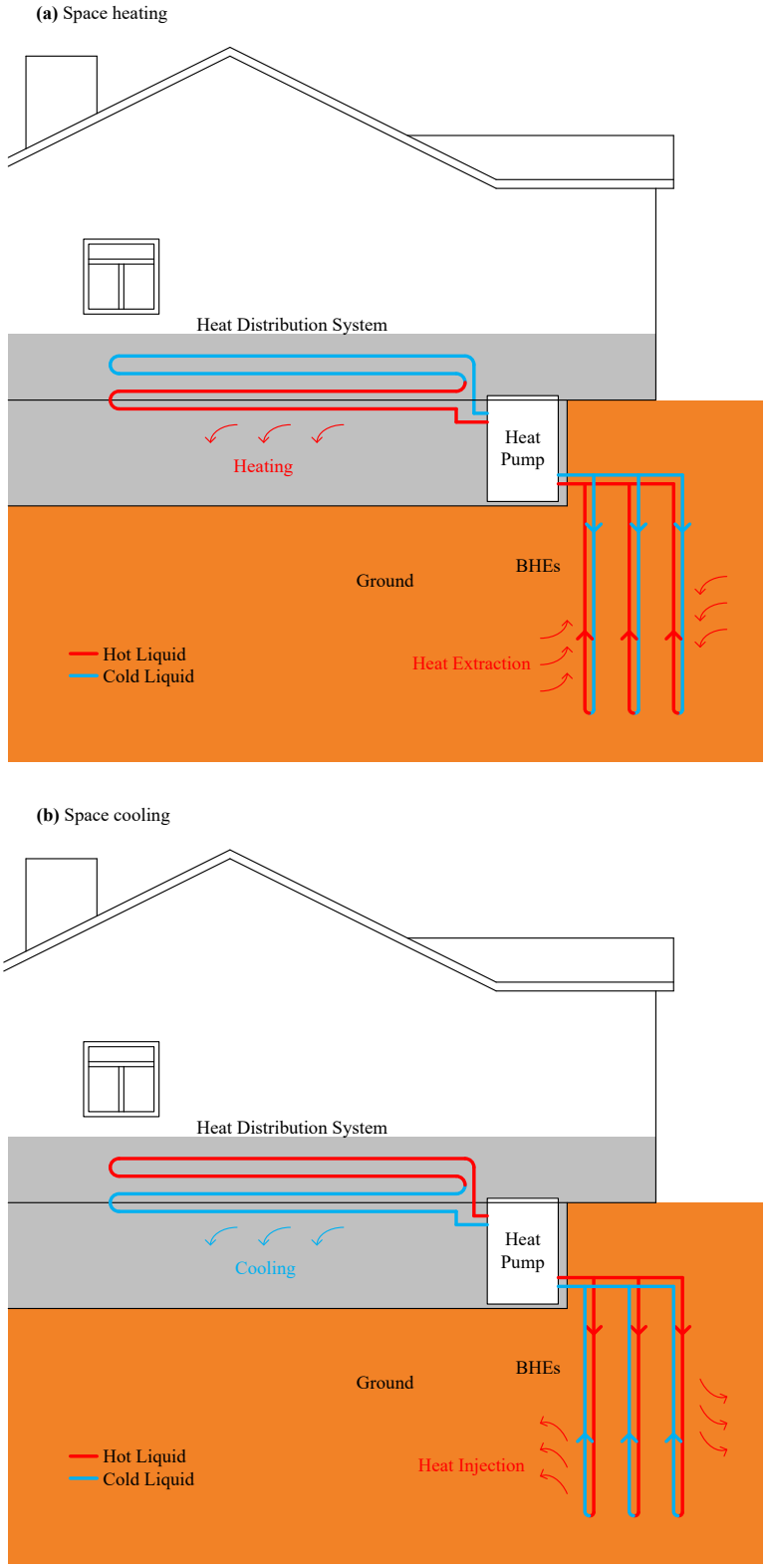

Figure 1. Schematics of a GSHP system for space (a) heating and (b) cooling.

To evaluate the long-term performance of BHE, an approach using the *g*-function (also known as thermal response factor) is widely accepted. The *g*-function is determined by the following relationship [17]:

$$\Delta T = T_b - T_0 = \frac{q_l}{2\pi k} \times g(x_1, x_2, \cdots) \quad (1)$$

where, T_b [K] is the borehole wall temperature; T_0 [K] is the undisturbed ground temperature; q_l [Wm^{-1}] is the rate of heat production or withdrawal per unit length; k [$Wm^{-1}K^{-1}$] is the ground thermal conductivity; $g(x_1, x_2, \cdots)$ is the *g*-function; and x_1, x_2 are several non-dimensional parameters, such as non-dimensional time and non-dimensional borehole radius. The *g*-function is the non-dimensional temperature variation ($\overline{\Theta}$), averaged over the borehole wall surface, in response to a time-constant heat transfer rate in a single BHE [18, 19]:

$$g(x_1, x_2, \cdots) = \overline{\theta} = \frac{2\pi k \Delta T}{q_l} \quad (2)$$

The *g*-function approach is widely used because of two reasons. First, since the *g*-function is non-dimensional, it is convenient for a wide range of ground thermal properties and borehole geometries with equal non-dimensional parameters. For example,

the same *g*-function can be valid for boreholes with various lengths (*H*) and radiuses (r_b), as long as these boreholes have the same non-dimensional borehole radius (r_b/H). Second, *g*-functions can be computed to consider thermal interaction between multiple boreholes with the help of the spatial superposition principle [17, 20]. The temporal superposition principle can also be employed to consider the time-varying heat flux due to variations in cooling and heating loads of projects [19]. In this regard, the *g*-function methodology has been implemented commonly in GSHP design tools, such as GLHEPRO [21] and Earth Energy Designer (EED) [22]. Current available *g*-functions are obtained through numerical models [23-26], analytical models [27-32], or a combination of the two [17, 33]. In engineering practice, analytical models are generally favoured over numerical models for sizing, optimizing and simulating the BHE system [34-37]. Advantages to the analytical approach include (1) the flexibility for any BHE geometries and configurations, (2) the superior computational time with an acceptable accuracy, and (3) the simplicity for the designers [30, 38]. This research emphasizes on *g*-functions obtained from analytical models.

1.2. Problem definition

A review of existing analytical models for computing *g*-functions (see Ch. 2) shows that several simplifications were assumed in the development of the analytical models. These simplifications include, but are not limited to, (a) adiabatic top layer assumption, (b) purely heat conduction assumption, (c) constant ground surface temperature assumption, and (d) homogeneous ground assumption. The analytical models have also been further explored in the corresponding aspects to reflect myriad practical conditions in BHE

design: (a) buried depth [29, 39], (b) groundwater flow [30, 31], (c) ground surface temperature [32, 40], and (d) multiple ground layers [38, 41]. Among these aspects, the buried depth and groundwater flow are of particular importance in BHE design. These two aspects are briefly introduced as below.

Buried depth (D) is the distance from the ground surface to the starting point of the vertical BHEs (see Fig.2) [42]. This distance was taken as zero in some analytical solutions [27, 28, 30, 31]. However, buried depth varies in different geological environments and climates regions. In cold regions (e.g., Canada, Northern Europe), ground temperature can drop below the freezing point of groundwater [43]. Therefore, BHEs are normally buried deeper in cold regions than in warm regions to avoid the associated risk of freeze-thaw cycles in the seasonally frozen ground [44]. As the buried depth increases, the heat exchange between the ground surface and BHEs is diminished by the thermal resistance of the ground layer above the boreholes, yielding a lower thermal performance of BHEs [39, 45].

In addition to buried depth, another significant aspect in BHE design is groundwater flow. Groundwater is the water that exists in the pores in saturated ground, and it flows showing hydraulic gradients [46]. According to local geological and hydraulic conditions, groundwater flow rates vary from metres per year to metres per day [46]. Groundwater flow is found in many geological environments, and it can considerably change the temperature regime around the borehole [34, 47]. When groundwater exists, the heat exchange between the borehole and the ground is inherently coupled with gross heat advection by the movement of groundwater, providing a synergistic effect on the thermal

performance of BHEs. This synergistic effect can shorten the design length of BHEs without sacrificing performance [48-50].

In general, buried depth and groundwater flow both have certain influences on the long-term performance of BHE. However, no work has been done to incorporate their effects at the same time in an analytical model. To this end, a new solution of the analytical model is needed to offer a more accurate estimation of the *g*-function by taking the buried depth and groundwater flow into consideration.

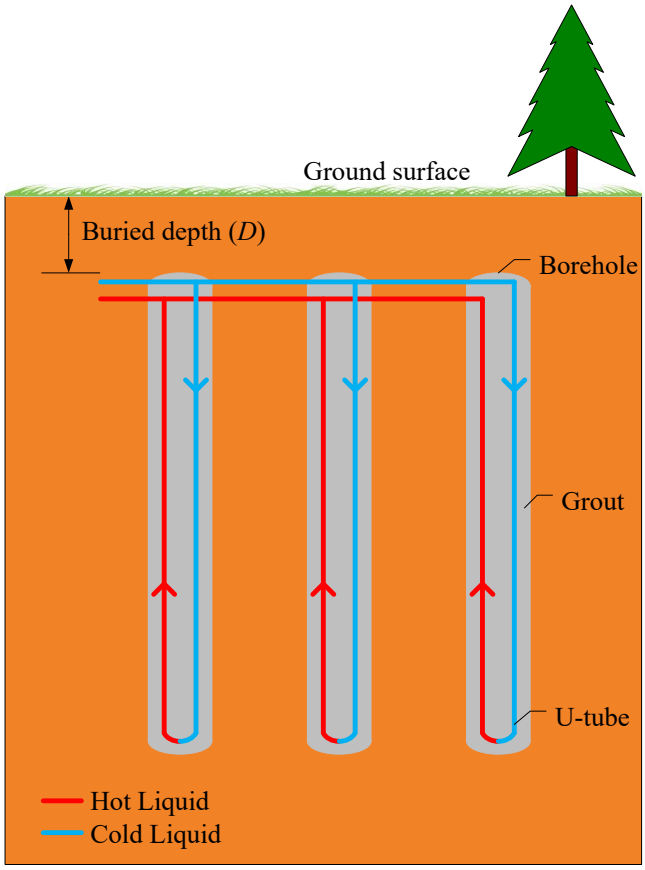

Figure 2. Schematic of borehole heat exchangers (BHEs).

1.3. Research objective

The overall objective of the present study is to develop a new analytical solution for computing *g*-functions in order to take account of the effects of buried depth and groundwater flow.

Besides, four sub-objectives are also identified:

i. Review analytical model for a single borehole;

ii. Verify the new derived analytical solution numerically;

iii. Elucidate the role of buried depth in BHEs design;

iv. Examine the thermal interactions within the borehole fields.

1.4. Thesis structure

The thesis is organized according to the objectives of this study and presented in seven chapters. This chapter (Ch. 1) introduce the background and defined the problem of this study, as well as the objectives.

Chapter 2 provides a comprehensive review of the analytical line source models for a single borehole, as well as the spatial superposition principle for multiple borehole field.

Chapter 3 proposed a new integral mean solution of the MFLS model that considers the effects of buried depth (MFLSD). This chapter also presents a three-dimensional (3D) finite element (FE) COMSOL model constructed using the software COMSOL Multiphysics for numerical verification.

Chapter 4 presents the numerical verification of MFLSD solution. This chapter also presents a sensitivity study of buried depth in the non-dimensional form.

Chapter 5 presents the investigation of the thermal interactions with borehole field.

Chapter 6 concludes the major findings from this work

Chapter 7 lists the major limitations of this work and suggests a direction for the further study.

2. Analytical models (Literature review)

Most analytical models for computing *g*-functions [28, 29, 39, 51] evolved from the line source theory [52]. The term "line source" refers to a continuous series of point heat sources along a straight line with a constant heat flux per unit length (q_l) [52]. In practice, the borehole can be assumed to be a line source because the radius of the borehole (e.g., r_b = 0.045 m) is tiny when compared with its length (e.g., H = 70 m) [27]. In this chapter, four analytical models have been briefly reviewed—the infinite line source model (ILS), the finite line source model (FLS), the moving infinite line source model (MILS), and the moving finite line source model (MFLS). Among these models, the ILS model is the earliest version of *g*-function; the FLS model is the current design theory implemented in commercial software (e.g., GLD2016 [53]); and the MILS model and the MFLS model are refined analytical models that include the effects of groundwater flow.

2.1. Infinite line source (ILS) model

Infinite line source (ILS) model is the earliest analytical model to calculate the heat transfer between a single borehole and its surrounding ground [20]. To apply the ILS model in the thermal analysis of BHE, the ground is regarded as an infinite, homogeneous and isotropic medium, in which the borehole is assumed as an infinite line source [18]. In the ILS model, the heat transfer is governed by the one-dimensional transient heat conduction equation in the radial direction [26, 52]:

$$\rho c \frac{\partial T}{\partial t} = k\left(\frac{\partial^2 T}{\partial r^2} + \frac{1}{r}\frac{\partial T}{\partial r}\right) \tag{3}$$

where T [°C] is the temperature of the medium, k [$Wm^{-1}K^{-1}$] is the ground thermal conductivity, ρc [$Jm^{-3}K^{-1}$] is the volumetric heat capacity of the medium, and r [m] is the radial distance to the line source.

If the line source starts releasing heat continuously at time zero, and if the medium has a uniform initial temperature (T_0), a mathematical solution of the ILS model (Ingersoll et al. [52]) gives the temperature variation (ΔT) at any later time (t) and any radius (r) around the line.

$$\Delta T_{ILS} = \frac{q_l}{2\pi k} \cdot \int_{r/\sqrt{4\alpha t}}^{\infty} \frac{e^{-\beta^2}}{\beta} d\beta \tag{4}$$

where $\beta = \frac{r}{\sqrt{4\alpha\left(t - t'\right)}}$, and $\alpha = k/\rho c$ [m^2s^{-1}] is the thermal diffusivity.

Introducing the exponential integral function $E_1\left(X\right) = \int_X^{\infty} \frac{e^{-t}}{t} dt$, which is a special function in mathematics, Carslaw and Jaeger [54] described Eq.(4) as:

$$\Delta T_{ILS} = \frac{q_l}{4\pi k} \cdot \int_{r^2/(4\alpha t)}^{\infty} \frac{e^{-\phi}}{\phi} d\phi = \frac{q_l}{4\pi k} \cdot E_1\left(\frac{r^2}{4\alpha t}\right) \tag{5}$$

where $\phi = r^2/\left(4\alpha\left(t-t'\right)\right)$.

At the time $t \geq 5r^2/\alpha$, the exponential integral $E_1\left(X\right)$ in Eq. (5) can be approximated as:

$$E_1\left(\frac{r^2}{4\alpha t}\right) = ln\left(\frac{4\alpha t}{r^2}\right) - \gamma \tag{6}$$

where γ donates the Euler's constant (approximating to 0.5772…).

Gehlin [47] reported that the natural logarithm approximation gives errors less than 10%. The maximum error drops to 2.5% for the time $t \geq 20r^2/\alpha$.

The ILS model is characterized by its simplicity [18]. However, these assumed simplifications may also restrict its applications. First, the pure conductive heat transfer assumption ignores the presence of groundwater flow that has considerable influence in the long-time period. Second, the infinite assumption neglects the heat transfer in the direction of the borehole axis (i.e., axial effect), including the heat conduction at the bottom and top of boreholes. As a result, the solutions of Eq. (4) and Eq. (5) are

inadequate for yearly simulation of BHEs system [27, 32]. Marcotte et al. [55] concluded that the borehole length could be 15% shorter when the axial effect is considered.

2.2. Finite line source (FLS) model

A step forward to the ILS model, the finite line source (FLS) model considers the borehole as a constant line source with a finite length to solve the governing equation of two-dimentional (radial and axial) transient heat conduction [56] in clindrycial coordinates (r, φ, z) as below:

$$\rho c \frac{\partial T}{\partial t} = k\left(\frac{\partial^2 T}{\partial r^2} + \frac{1}{r}\frac{\partial T}{\partial r} + \frac{\partial^2 T}{\partial z^2}\right) \tag{7}$$

In the FLS model, the ground is regarded as a semi-infinite medium by assuming that the interface between ambient air and ground surface is maintained at constant temperature (the same as the undisturbed ground temperature T_0).

Initially proposed by Eskilson [17], a general solution of the FLS model was later constructed by Zeng et al. [27]. Setting a virtual mirror sink above the ground surface, the constant temperature boundary condition at the surface is compiled by the symmetrical distribution of line heat source and sink. Then the temperature rise at a point of the surrounding ground can be obtained by integrating contributions of all the continuous point sources on the line heat source and sink [17, 27]:

$$\Delta T_{FLS} = \frac{q_l}{4\pi k} \cdot \int_{D}^{H+D} \left[\frac{erfc\left(\frac{\sqrt{r^2 + (z-z')^2}}{\sqrt{4\alpha t}} \right)}{\sqrt{r^2 + (z-z')^2}} - \frac{erfc\left(\frac{\sqrt{r^2 + (z+z')^2}}{\sqrt{4\alpha t}} \right)}{\sqrt{r^2 + (z+z')^2}} \right] dz' \qquad (8)$$

where H [m] is the borehole length, D [m] is the buried depth, z' is the coordinate of the point source, and $erfc(X) = \frac{2}{\sqrt{\pi}} \int_{X}^{\infty} e^{-t^2} dt$ is the complementary error function in mathematics.

In Eskilson's original work [17], it concluded that the exact value of buried depth (D) is not important for a fixed active borehole length (H), since only small temperature variations (i.e., 0.1 °C) were found among several numerical simulations for buried depth of 2 m to 8 m. However, the other used input parameters were not reported.

The temperature variation is only given at a single point by Eq. (8). To estimate the average borehole wall temperature variation, the FLS solution by Zeng et al. [27] requires one additional integration at the borehole radius (r_b) over the borehole length (H).

$$\overline{\Delta T_{FLS}} = \frac{1}{H} \cdot \int_{0}^{H} \Delta T_{FLS} dz \qquad (9)$$

Accordingly, this double integration results in a remarkable increase of computational efforts. Then Lamarche and Beauchamp [28] presented another expression for the FLS model that simplifies the FLS solution by Zeng et al. [27] from a double integral into a single integral. This simplification considerably reduced the computational time by a factor of thousand times [28]. The Lamarche and Beauchamp's expression [28] for integrated average temperature variation is:

$$\overline{\Delta T_{FLS}} = \frac{q_l}{2\pi k} \cdot \left[\int_r^{\sqrt{r^2+H^2}} \frac{erfc\left(\frac{\gamma}{\sqrt{4\alpha t}}\right)}{\sqrt{\gamma^2 - r^2}} d\gamma - A - \int_{\sqrt{r^2+H^2}}^{\sqrt{r^2+4H^2}} \frac{erfc\left(\frac{\gamma'}{\sqrt{4\alpha t}}\right)}{\sqrt{\gamma'^2 - r^2}} d\gamma' - C \right] \tag{10}$$

where $\gamma = \sqrt{r^2 + (z - z')^2}$, $\gamma' = \sqrt{r^2 + (z + z')^2}$ and

$$\begin{aligned} A &= \int_r^{\sqrt{r^2+H^2}} erfc\left(\frac{\gamma}{\sqrt{4\alpha t}}\right) d\gamma \\ C &= \frac{1}{2} \cdot \left[\int_r^{\sqrt{r^2+H^2}} erfc\left(\frac{\gamma'}{\sqrt{4\alpha t}}\right) d\gamma' - \int_{\sqrt{r^2+H^2}}^{\sqrt{r^2+4H^2}} erfc\left(\frac{\gamma'}{\sqrt{4\alpha t}}\right) d\gamma' \right] \end{aligned} \tag{11}$$

Bandos et al. [32] also presented a single integral expression for approximating the FLS solution. Taking account for the air temperature fluctuation at the ground surface, this approximation was used to estimate the ground thermal conductivity from the TRT data. The estimation demonstrated that the finite length correction of the borehole yields a

lower estimated value of the ground thermal conductivity and improves the accuracy of the evaluation [57]. Moreover, this approximation, as shown below, was implemented in commercial design tool GLD2016 as the current design approach [53].

$$\overline{\Delta T_{FLS}} = \frac{q_l}{4\pi k} \cdot \int_{r/\sqrt{4\alpha t}}^{\infty} \frac{e^{-\beta^2}}{\beta} \cdot \left[4erf\left(\frac{H\beta}{r}\right) - 2erf\left(\frac{2H\beta}{r}\right) - \frac{r}{H\beta\sqrt{\pi}} \cdot \left(3 + exp\left(-\frac{4H^2\beta^2}{r^2}\right) - 4\,exp\left(-\frac{H^2\beta^2}{r^2}\right)\right)\right] d\beta \tag{12}$$

where $erf(X) = 1 - erfc(X)$ is the error function in mathematics.

More recently, Claesson and Javed [29] reformulated the FLS solution by changing the order of the integration. Zeng et al. [27] and Lamarche and Beauchamp [28] integrated the point heat source in the time domain first, and then the solutions (Eq. (8) and (10)) were given in a form of a single integral in the space domain. On the contrary, Claesson and Javed [29] integrated the point heat source in the space domain first, and then the solution was given in a form of a single integral in the time domain. In this way, the FLS solution by Claesson and Javed [29] took the buried depth (*D*) into consideration

$$\overline{\Delta T_{FLS}} = \frac{q_l}{4\pi k} \cdot \int_{1/\sqrt{4\alpha t}}^{\infty} e^{-r^2 s^2} \cdot \frac{Fun(Hs, Ds)}{Hs^2} ds \tag{13}$$

where $s = \frac{1}{\sqrt{4\alpha(t-t')}}$ and

$$Fun(X,Y) = 2ierf(X) + 2ierf(X+2Y) - ierf(2X+2Y) - ierf(2Y)$$

$$ierf(X) = \int_0^X erf(Y)dY = Xerf(X) - \frac{1}{\sqrt{\pi}}\left(1 - e^{-X^2}\right) \tag{14}$$

The FLS model has considered the finite length of the borehole, through which the effects of axial heat conduction has been taken into account. In particular, the axial heat conduction accelerates the heat exchange at the bottom of the borehole and transfers the imbalance heat of extraction and injection on a year-round basis to the ambient air through the ground surface [27, 30]. However, the FLS model is still a solution to the purely heat conductive problem, which neglects the heat advection by groundwater flow.

2.3. Moving infinite line source (MILS) model

The moving infinite line source model (MILS) was explored by Sutton et al. [58] and Diao et al. [46] to account for the convective heat transported by the moving water. In MILS model, the heat transfer is composed of (1) heat conduction through the solid and water in the pores and (2) the heat advection through the flowing groundwater. Based on moving heat source theory [59], the heat conduction-advection equation (Eq. (15)) was established using the effective thermal transfer velocity (U) in place of the moving speed of the heat source. Assuming that the groundwater flows parallel to the ground surface in the x-direction, the two-dimensional (xy coordinates plane) heat conduction-advection of a moving line source in a saturated porous medium can be expressed as follow [46]:

$$\rho c\frac{\partial T}{\partial t}=k\left(\frac{\partial^2 T}{\partial x^2}+\frac{\partial^2 T}{\partial y^2}\right)-u_d\rho_w c_w\frac{\partial T}{\partial x}\ \Rightarrow\ \frac{\partial T}{\partial t}=\alpha\left(\frac{\partial^2 T}{\partial x^2}+\frac{\partial^2 T}{\partial y^2}\right)-U\frac{\partial T}{\partial x} \tag{15}$$

where u_d [ms^{-1}] denotes the uniform groundwater velocity which can be determined using Darcy's law, $\rho_w c_w$ [Jm^{-3}K^{-1}] is the volumetric heat capacity of the groundwater and $U=u_d\rho_w c_w/(\rho c)$ [ms^{-1}] is the effective thermal transfer velocity.

Diao et al. [46] and Sutton et al. [58] solved the partial differential Eq. (15) for an infinite moving line using the Green's function method [60]:

$$\overline{\Delta T_{MILS}}=\frac{q_l}{4\pi k}\cdot exp\left(\frac{Ux}{2\alpha}\right)\cdot\int_{r^2/(4\alpha t)}^{\infty}\frac{1}{\phi}\cdot exp\left(-\phi-\frac{U^2\left(x^2+y^2\right)}{16\alpha^2\phi}\right)d\phi \tag{16}$$

The MILS model has incorporated the effect of moving groundwater. However, results produced by the MILS model usually overestimate the long-term temperature response (years and decades), because the axial effects are not taken into account [30]. This is a common disadvantage for all the analytical models that adopt the infinite assumption.

2.4. Moving finite line source (MFLS) model

For long-term simulation of BHEs operation, both the axial heat conduction and groundwater flow can considerably change the temperature regime around the borehole. As a result, the moving finite line source (MFLS) model was developed to take into account both effects [30]. The governing equation of the three-dimensional heat conduction-advection in porous media is described as follow [61]:

$$\rho c \frac{\partial T}{\partial t} = k\left(\frac{\partial^2 T}{\partial x^2} + \frac{\partial^2 T}{\partial y^2} + \frac{\partial^2 T}{\partial z^2}\right) - u_d \rho_w c_w \frac{\partial T}{\partial x} \tag{17}$$

Using the same theory as the MILS model and applying a methodology similar to the FLS model, Molina-Giraldo et al. [30] proposed a general solution of the MFLS model which turns out to be:

$$\overline{\Delta T_{MFLS}} = \frac{q_l}{2\pi k} \cdot exp\left(\frac{Ux}{2\alpha}\right) \cdot \left[\int_0^H \frac{f(x,y,z,t)}{4\gamma} dz' - \int_{-H}^0 \frac{f(x,y,z,t)}{4\gamma} dz'\right]$$

$$f(x,y,z,t) = exp\left(-\frac{U\gamma}{2\alpha}\right) \cdot erfc\left(\frac{\gamma - Ut}{\sqrt{4\alpha t}}\right) + exp\left(\frac{U\gamma}{2\alpha}\right) \cdot erfc\left(\frac{\gamma + Ut}{\sqrt{4\alpha t}}\right) \tag{18}$$

Similar to the FLS solution of Zeng et al. (Eq. (8)), Eq. (18) needs integrating itself over the borehole length and the borehole circumference for the average borehole wall temperature. Therefore, inspired by Lamarche and Beauchamp [28], Tye-Gingras and Gosselin [31] reformulated the triple integral formulation to an alternative single integral expression:

$$\overline{\Delta T_{MFLS}} = \frac{q_l}{2\pi k} \cdot I_0\left(\frac{rU}{2\alpha}\right) \cdot \left(A_1 + C_1 + C_2\right) \tag{19}$$

where $I_0\left(X\right)$ is the modified zero-order Bessel function of the first kind and

$$A_1 = \frac{1}{2} \int_r^{\sqrt{r^2+H^2}} \left(-1 + \frac{1}{\sqrt{\gamma^2 - r^2}}\right) \cdot f\left(x,y,z,t\right) d\gamma$$

$$C_1 = \frac{1}{4} \int_r^{\sqrt{r^2+4H^2}} f\left(x,y,z,t\right) d\gamma \tag{20}$$

$$C_2 = \frac{1}{2} \int_r^{\sqrt{r^2+4H^2}} \frac{1}{\sqrt{\gamma^2 - r^2}} \cdot f\left(x,y,z,t\right) d\gamma$$

Rivera et al. [62] also proposed an alternative expression to describe the integrated average temperature variation ($\overline{\Delta T_{MFLS}}$) at the borehole wall ($r = r_b$). The expression was developed based on the FLS approximation given by Bandos et al (Eq. (12))

$$\overline{\Delta T_{MFLS}} = \frac{q_l}{8\pi k} \cdot I_0\left(\frac{rU}{2\alpha}\right) \cdot \int_{r^2/(4\alpha t)}^{\infty} \frac{1}{\xi} \cdot exp\left(-\xi - \frac{U^2 r^2}{16\alpha^2 \xi}\right) \cdot \left[4erf\left(\frac{H\sqrt{\xi}}{r}\right) - 2erf\left(\frac{2H\sqrt{\xi}}{r}\right) - \frac{r}{H\sqrt{\pi\xi}} \cdot \left(3 + exp\left(-\frac{4H^2\xi}{r^2}\right) - 4\,exp\left(-\frac{H^2\xi}{r^2}\right)\right)\right] d\xi \quad (21)$$

where $\xi = \beta^2$.

One step to the FLS and MILS models, the MFLS model incorporated the effects of groundwater flow and axial heat conduction at the same time. However, the current available MFLS model negelectd the buried depth (*D*) which also has considerable influence in the long-term simulation of the BHEs operation.

In brief, this chapter introduced four analytical models for a single borehole. In Appendix A, a comparison was made between these models to evaluate the effects of groundwater flow and axial conduction.

2.5. Superposition principle for borehole fields

These aforementioned analytical models for a single borehole have provided a foundation for thermal analysis of a multiple borehole field [46]. As stated in Ch.1, the principle of superposition can be applied in to consider thermal interaction between multiple boreholes [17, 25, 28, 31, 63]. In practical applications, multiple BHEs are common in large-scale commercial buildings that have high energy demands. In this case, temperature variations of multiple BHEs should be more significant than the one of

single BHE due to the thermal interaction between boreholes [64]. A simplified approach to obtain the temperature variations at any location in a multiple borehole field is superposing the contribution of each individual line source. For a BHEs field composed of N boreholes (see Fig. 3), the mean temperature variation on a certain borehole wall (i.e., borehole i) is given by:

$$\overline{\Delta T_i} = \sum_{j=1}^{N} \overline{\Delta T_{j \to i}} \tag{22}$$

where $\overline{\Delta T_{j \to i}}$ is the thermal effect of borehole j on the borehole i.

The overall temperature variation over the field is then computed as following:

$$\overline{\Delta T_N} = \frac{1}{N} \sum_{i=1}^{N} \sum_{j=1}^{N} \overline{\Delta T_{j \to i}} \tag{23}$$

Then a new g-function for a particular borehole configuration can be computed using Eq. (2) while accounting for the thermal interaction among boreholes.

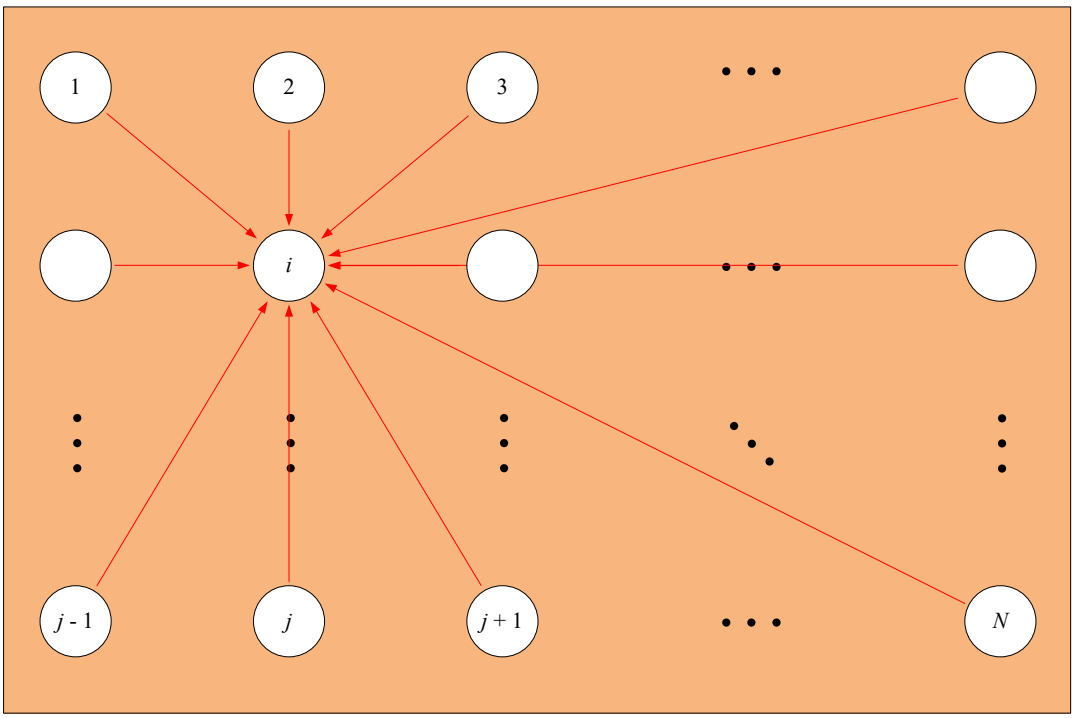

Figure 3. Schematic (plan view) for the thermal interaction on a specific borehole *i* in a multiple borehole field with *N* boreholes.

3. Methodology

In this section, a new analytical solution of the MFLS model (MFLSD) is presented. Inspired by the FLS solution of Claesson and Javed [29], the MFLSD solution was derived in a single integral form with consideration of the buried depth. The spatial superposition principle was employed to computing new *g*-functions for multiple borehole field. To numerically verify the MFLSD solution and the new *g*-functions, a three-dimensional (3D) finite element (FE) model was constructed using the software COMSOL Multiphysics for numerical verification. The 3D-FE solution solved the same heat transfer problem as the MFLSD solution using the same input parameters from a real geoexchange project in Edmonton, Alberta, Canada. The discrepancy between the two solutions is evaluated using the mean absolute error (MAE) and the root mean square deviation (RMSD). A one percent (1%) difference is employed as a criterion to decide whether the effects of buried depth are negligible. When the discrepancy between the MFLSD solution and the MFLS solution is greater than 1%, the *g*-function must be computed using MFLSD solution to include the effects of buried depth. A general flowchart is shown as below:

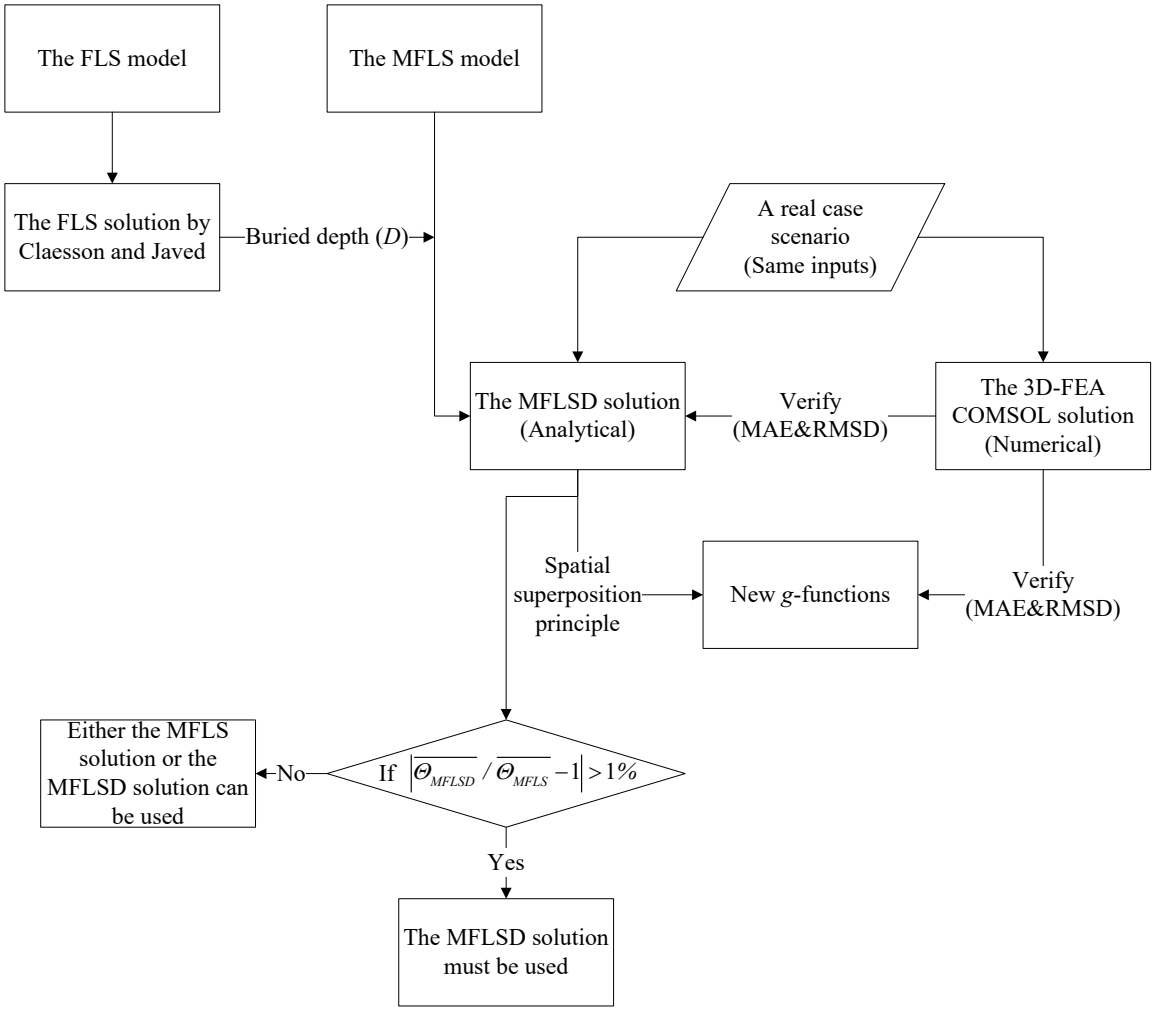

Figure 4. A flowchart showing the overall methodology.

3.1. Moving finite line source model that includes buried depth (MFLSD) – a new solution

Claesson and Javed [29] provided a two-dimensional (radial and axial) mathematical solution for geothermal analysis. The model gives the average temperature variation over the length of a line source at a distance below a constant temperature surface in the axial direction and at a radial distance from the line source. Based on their mathematical

approach, the MFLS solution was modified in this study to calculate the average borehole wall temperature variation ($\overline{\Delta T}$), taking buried depth into account.

Three common simplifying assumptions are made to develop this new MFLS solution, these assumptions are consistent with the work of Tye-Gingras and Gosselin [31]:

a. The groundwater is parallel to the ground in the *x*-direction with a uniform Darcy velocity u_d;

b. Local thermal equilibrium (LTE) is considered (i.e., the groundwater temperature is the same as the ground temperature at any point), which is a commonly used hypothesis for heat transfer in porous media[65]. In a macroscopic scale, LTE is valid because the temperatures of water and solid vary slowly in time and space, and the difference between them is very small [66];

c. All the thermal and hydraulic properties are not affected by temperatures.

The governing equation of the heat conduction-advection in porous media is given as follows [61]:

$$\rho c \frac{\partial T}{\partial t} = k\left(\frac{\partial^2 T}{\partial x^2} + \frac{\partial^2 T}{\partial y^2} + \frac{\partial^2 T}{\partial z^2}\right) - u_d \rho_w c_w \frac{\partial T}{\partial x} \tag{24}$$

The solution of the partial differential equation (Eq. (24)) for the temperature difference at any later time (t) and any arbitrary point (x, y, z) of a continuous point source at coordinate (0, 0, z') in a semi-infinite porous media is given by the Green's function [60]:

$$\Delta T = \frac{q_l}{8\rho c\left(\pi\alpha\right)^{3/2}} \cdot \int_0^t \frac{1}{\left(t - t'\right)^{3/2}} \cdot exp\left(- \frac{\left(x - U\left(t - t'\right)\right)^2 + y^2 + \left(z - z'\right)^2}{4\alpha\left(t - t'\right)} \right) dt' \qquad (25)$$

Using the substitution $s = \frac{1}{\sqrt{4\alpha\left(t - t'\right)}}$, then $ds = \frac{\alpha}{4\left(\alpha\left(t - t'\right)\right)^{3/2}} dt'$, and integrating by parts, the solution becomes:

$$\Delta T = \frac{q_l}{4\pi k} \cdot exp\left(\frac{xU}{2\alpha}\right) \cdot \int_{1/\sqrt{4\alpha t}}^{\infty} exp\left(- \frac{U^2}{16\alpha^2 s^2} - \left(x^2 + y^2\right)s^2 - \left(z - z'\right)^2 s^2 \right) ds \qquad (26)$$

Then, the Cartesian coordinates (x, y, z) are converted to cylindrical coordinates (r, φ, z):

$$\Delta T = \frac{q_l}{4\pi k} \cdot exp\left(\frac{rU}{2\alpha} cos\left(\varphi\right)\right) \cdot \int_{1/\sqrt{4\alpha t}}^{\infty} exp\left(- \frac{U^2}{16\alpha^2 s^2} - r^2 s^2 - \left(z - z'\right)^2 s^2 \right) ds \qquad (27)$$

where $\varphi = cos^{-1}\left(\frac{x}{r}\right)$; and $r = \sqrt{x^2 + y^2}$ is the radial distance to the line source.

As shown in Fig. 5, a constant temperature surface can be set up by the method of images [27]. After that, temperature variation at any point is obtained from the spatial integration of the point sources and point sinks along the z-axis over the heat source length $D < z < D + H$;

$$\Delta T = \frac{q_l}{4\pi k} \cdot exp\left(\frac{rU}{2\alpha} cos(\varphi)\right) \cdot \int_{1/\sqrt{4\alpha t}}^{\infty} exp\left(-\frac{U^2}{16\alpha^2 s^2} - r^2 s^2\right) \cdot \frac{2}{\sqrt{\pi}} \cdot \int_{D}^{D+H} \left[exp\left(-(z-z')^2 s^2\right) - exp\left(-(z+z')^2 s^2\right)\right] dz' ds \tag{28}$$

One additional integration is required to estimate the average temperature variation along the borehole length. Then, the integrated average temperature variation over the heat source length is represented as a triple integral:

$$\overline{\Delta T} = \frac{q_l}{4\pi k} \cdot exp\left(\frac{rU}{2\alpha} cos(\varphi)\right) \cdot \int_{1/\sqrt{4\alpha t}}^{\infty} exp\left(-\frac{U^2}{16\alpha^2 s^2} - r^2 s^2\right) \cdot \frac{2}{H\sqrt{\pi}} \cdot \int_{D}^{D+H} \int_{D}^{D+H} \left[exp\left(-(z-z')^2 s^2\right) - exp\left(-(z+z')^2 s^2\right)\right] dz' dz ds \tag{29}$$

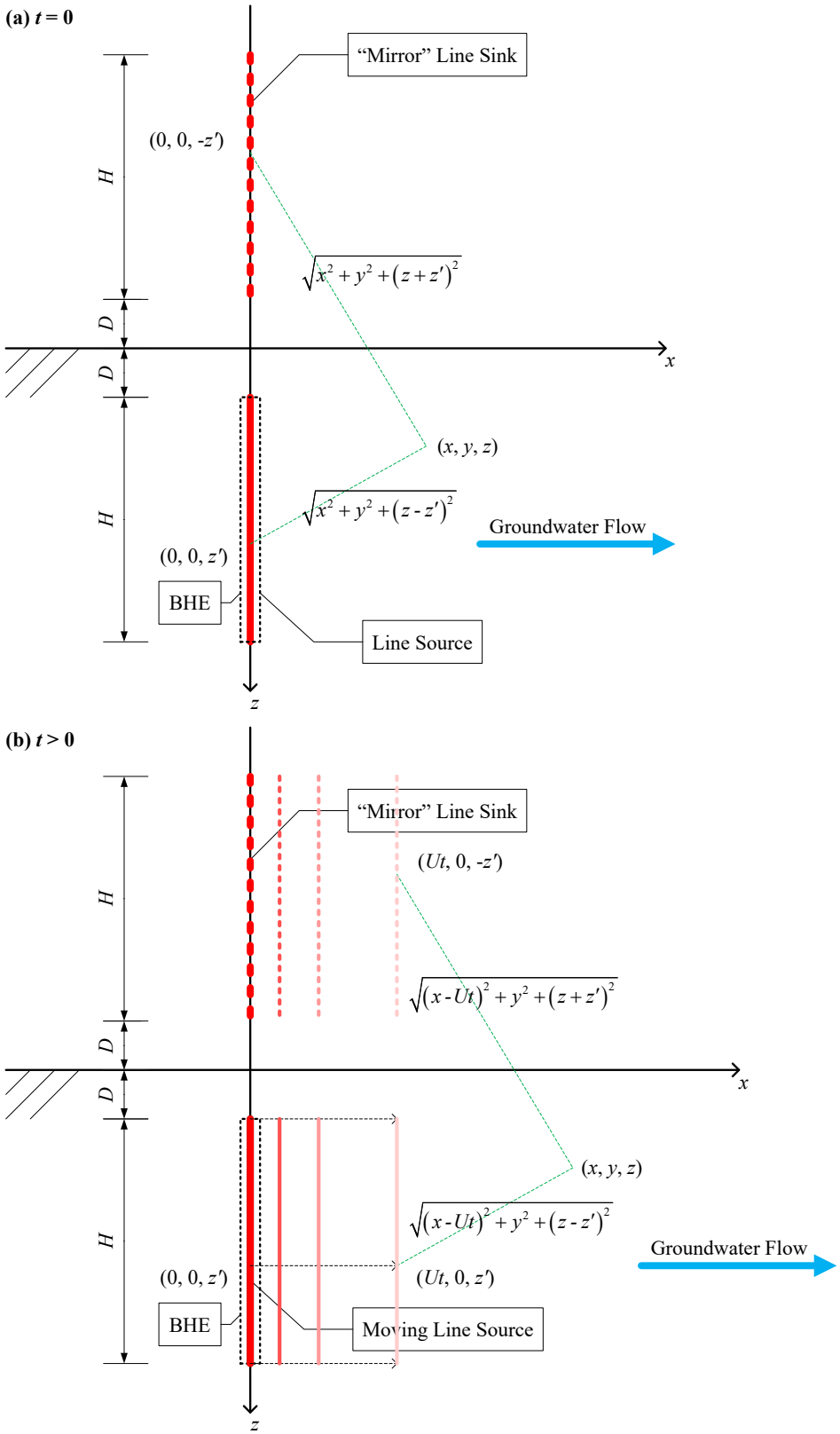

Figure 5. Schematics of the MFLSD solution.

Referring to the work of Claesson and Javed [29], a solution to the double integration part of Eq. (29) is provided as

$$\overline{\Delta T} = \frac{q_l}{4\pi k} \cdot exp\left(\frac{rU}{2\alpha} cos(\varphi) \right) \cdot \int_{1/\sqrt{4\alpha t}}^{\infty} exp\left(-\frac{U^2}{16\alpha^2 s^2} - r^2 s^2 \right) \cdot \frac{Fun(Hs, Ds)}{Hs^2} ds \qquad (30)$$

The average temperature variation, Eq. (30), can be integrated over the borehole circumference at the borehole radius (where $r = r_b$),

$$\overline{\Delta T} = \frac{q_l}{4\pi k} \cdot I_0\left(\frac{rU}{2\alpha} \right) \cdot \int_{1/\sqrt{4\alpha t}}^{\infty} exp\left(-\frac{U^2}{16\alpha^2 s^2} - r^2 s^2 \right) \cdot \frac{Fun(Hs, Ds)}{Hs^2} ds \qquad (31)$$

Both Eq. (30) and (31) can be non-dimensionalized to reduce the number of independent variables. Non-dimensional variables are introduced: $\overline{\Theta_{MFLS}} = \frac{2\pi k \Delta T}{q_l}$, $R_b = \frac{r_b}{H}, d = \frac{D}{H}$, Fourier number $Fo = \frac{\alpha t}{H^2}$ and Peclet number $Pe = \frac{UH}{\alpha}$. Both Eq. (30) and (31) can be expressed as

$$\overline{\Theta_{MFLS}}\left(R_b,\varphi,Fo,Pe,d\right)=$$
$$\frac{1}{2}\cdot exp\left(\frac{R_b Pe}{2}cos\left(\varphi\right)\right)\cdot\int_{1/\sqrt{4Fo}}^{\infty}exp\left(-\frac{Pe^2}{16s^2}-{R_b}^2s^2\right)\cdot\frac{Fun\left(s,d\cdot s\right)}{s^2}ds \quad (32)$$

$$\overline{\Theta_{MFLS}}(R_b,Fo,Pe,d)=$$
$$\frac{1}{2}\cdot I_0\left(\frac{R_b Pe}{2}\right)\cdot\int_{\frac{1}{\sqrt{4Fo}}}^{\infty}exp\left(-\frac{Pe^2}{16s^2}-{R_b}^2s^2\right)\cdot\frac{Fun(s,d\cdot s)}{s^2}ds \quad (33)$$

Eq. (33) gives the non-dimensional average temperature variation over a borehole wall surface due to its own heat load. In a BHE field containing multiple boreholes, the spatial superposition technique must be performed to compute the overall mean temperature variation of the whole field. To apply the spatial superposition principle, the heat transfer rate was normally assumed to be equal for all boreholes [28, 29]. Then, the thermal interaction effect of N boreholes on the borehole i becomes [31]

$$\overline{\Theta_i}\left(R_b,Fo,Pe,d\right)=\overline{\Theta_{MFLS}}\left(R_b,Fo,Pe,d\right)+\sum_{j=1\ \&\ j\neq i}^{N}\overline{\Theta_{j\to i}}\left(R_{j\to i},\varphi_{j\to i},Fo,Pe,d\right) \quad (34)$$

where, $\overline{\Theta_{j\to i}}$ is the thermal effect of borehole j on the borehole i in non-dimensional form, and

$$R_{j\to i}=\frac{1}{H}\sqrt{\left(x_j-x_i\right)^2+\left(y_j-y_i\right)^2}$$

$$cos\left(\varphi_{j\to i}\right)=\frac{x_i-x_j}{R_{j\to i}} \tag{35}$$

Then, the overall mean temperature response over the BHEs field (or *g*-function) for the MFLS solution is computed following

$$\begin{aligned} g_{MFLSD}\left(R_b,Fo,Pe,d,BHEs\ Configuration\right)&=\overline{\Theta_N}\left(R_b,Fo,Pe,d\right)\\ &=\frac{1}{N}\sum_{i=1}^{N}\overline{\Theta_i}\left(R_b,Fo,Pe,d\right)\end{aligned} \tag{36}$$

3.2. Implementing the MFLSD and numerical model through a real scenario

Validating the MFLSD solution requires comparison with established methods or data. Due to a lack of long-term physical monitoring data from a GSHP system, a numerical verification method is necessary. For the verification of the MFLSD solution, a test case is designed based on a real geoexchange system project in Edmonton. As shown in Table 1, a typical borehole used in a real geoexchange system project in Edmonton was chosen. The borehole length, buried depth and radius are 70 m, 2 m, and 0.04595 m, respectively. The influence of different buried depths was further examined. Guided by the Eskilson's

original work [17], two other values of buried depth (D = 0 m and 8 m) were selected for the study. The borehole spacing (B) selected in the project is 7.6 m. To reduce the thermal interference between individual boreholes with a small footprint, ASHRAE (American Society of Heating, refrigerating and Air-Conditioning Engineer [15]) recommended a borehole spacing from 6 m to 8 m. These two values of borehole spacing were also selected for the study.

The thermal properties were obtained from an in-situ thermal conductivity test from the local project [67]. The tested undisturbed ground temperature (T_0) is 6 °C, the thermal conductivity (k) is 1.59 $Wm^{-1}K^{-1}$, and the thermal diffusivity of the borehole (α) is 6.944 $\times 10^{-7}$ m^2s^{-1}. The volumetric heat capacity of the bulk porous medium (ρc) is 2.290 x 10^6 $Jm^{-3}K^{-1}$. A transient study was set for a sufficiently long time, from 20 hours (about Fo = 10^{-5}) to 100 years (about Fo = 0.5), to verify the MFLSD solution. For 100-year continuous simulates, the heat injection rate was kept at q_l = 56 Wm^{-1} which is the expected peak load on the U-tubes for the project.

The hydraulic condition was not tested in the project; however, a common assumption is made that groundwater is in the x-direction and parallel to the ground surface. Molina-Giraldo et al. [30] concluded that the influence of groundwater flow becomes non-negligible for Pe > 1.2. In our case, when D = 0 m, a preliminary analysis (Appendix. A.) shows that the influence of groundwater flow on the result is greater than 1% after a 1000-year continuous operation for Pe > 1.87. Hence, a scenario was defined with a uniform velocity at $u_d = 4\times10^{-8}$ ms^{-1} (or Pe = 7.5) to represent the heat conduction-

advection condition. In comparison, another scenario was defined at $u_d = 0$ ms^{-1} (or Pe = 0) for the conduction-dominated condition.

Table 1. Parameters used in the calculations [67].

Parameter	Value
Length of the borehole (H)	70 m
Borehole radius (r_b)	0.04595 m
Thermal conductivity ground (k)	1.59 Wm^{-1}K^{-1}
Thermal diffusivity of the ground (α)	6.944×10^{-7} m^{2}s^{-1}
Volumetric heat capacity-ground (ρc)	2.290×10^6 Jm^{-3}K^{-1}
Volumetric heat capacity-water ($\rho_w c_w$) at 6 °C	4.200×10^6 Jm^{-3}K^{-1}

Finally, a customized MATLAB code was employed, to calculate the mathematical solutions for the average borehole wall temperature variation ($\overline{\Delta T}$). For the evaluation of a single integral, the MATLAB *integral* function with a tolerance of 10^{-12} was used. All calculations were performed on an Intel Xeon-E3, 3.10 GHz processor with 64 GB RAM.

3.3. Numerical model for verification

Similar to many previous researchers (e.g. [38, 55-57]), a finite element analysis in COMSOL Multiphysics was used for this numerical verification Fig. 6 shows a

representation of the 3D-FE COMSOL model. A symmetrical boundary condition was applied to reduce the domain size by half. Every single borehole was represented by a cylinder aligned with the *z*-axis, and its surrounding ground was built as a water saturated porous medium with constant thermal properties. The model becomes more complex in a multiple borehole field. As shown in Fig. 7, a simple rectangle configuration of 3 × 2 boreholes with an equal borehole spacing (*B*) was selected for the multiple borehole study. The same borehole configuration has been used by many other researchers for BHEs modelling [24, 26, 39, 46, 68]. The boundary conditions were assigned according to the assumptions made for the analytical model. A constant continuous heat flux (q_l) of 56 Wm^{-1} of was applied along the length of the BHE. A uniform groundwater flow was assigned throughout the entire domain aligned with the *x*-axis. Moreover, a uniform initial temperature of 6 °C was assigned to the entire domain to represent undisturbed ground temperature (T_0). The top boundary was at a fixed temperature at the same values as the undisturbed ground temperature to represent constant ground surface temperature. Borehole geometries and thermal properties are the same as in the real case scenario.

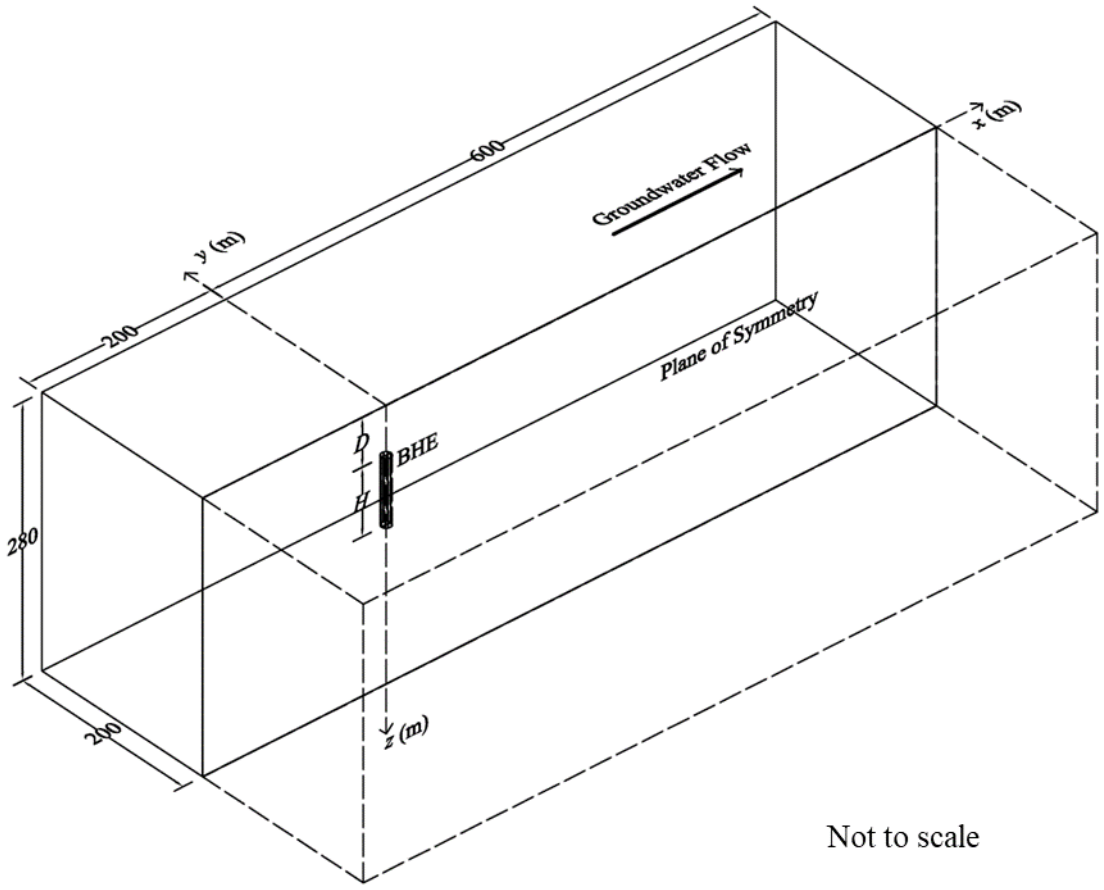

Figure 6. 3D-FE COMSOL model used for numerical verification of a single borehole.

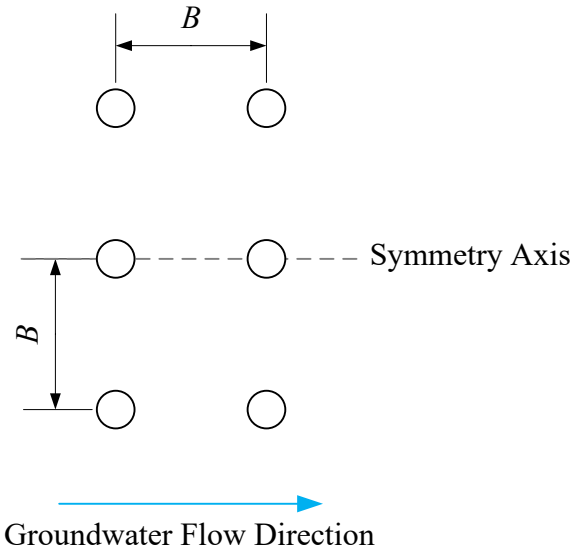

Figure 7. Schematic of a multiple borehole field of 3 × 2 boreholes with an equal borehole spacing (B).

A preliminary analysis was done to ensure that the simulation results are unaffected by the extension of the model domain and the size of elements. More detailed information is provided in Appendix B. After the preliminary analysis, a model was constructed with a horizontal domain of (x = 800 m) × (y = 200 m) and a thickness of (z = 280m). At the selected domain size, temperature changes at the external boundaries were less than 0.004 °C at the end of the simulations. The reliability of the domain size was also verified by comparing the average temperature at the borehole wall; the average temperature had a relative difference of less than 1% in the last extension. In addition, the mesh was generated using free tetrahedral elements. In order to have a more accurate temperature variation at the borehole wall, extremely fine (0.018 m) elements were meshed close to the borehole, and coarser elements (20 m) were meshed further out. The mesh geometry with about two million (2,000,000) elements was selected to ensure the mesh independent. When the number of elements of the domain doubled from about one million to two million, the maximum difference of the $\overline{\Delta T}$ was about 0.04% in the considered time domain.

To calculate the discrepancy between the MFLSD solution and the 3D-FE COMSOL solution, the MAE and RMSD were computed over the given time period from 20 hours to 100 years. MAE and RMSD are two of the most well-known and commonly accepted estimators that tell how much spread there is for the solutions in the vertical direction [69]. In our case, the MAE represents the average magnitude of the differences between the $\overline{\Theta}$ predicted from MFLSD solution and the $\overline{\Theta}$ observed from the FE COMSOL solution:

$$MAE = \frac{\sum_{i=1}^{N} \left| \overline{\Theta_A}(Fo_i) - \overline{\Theta_C}(Fo_i) \right|}{N} \tag{37}$$

And the RMSD represents the standard deviation of that differences:

$$RMSD = \sqrt{\frac{\sum_{i=1}^{N} \left(\overline{\Theta_A}(Fo_i) - \overline{\Theta_C}(Fo_i) \right)^2}{N}} \tag{38}$$

The acceptable values for MAE and RMSD are decided for each specific case [70]. Molina-Giraldo et al. [30] accepted a RMSD of 0.03 °C with respect to ΔT (equivalent to RMSD = 0.02 with respect to $\overline{\Theta}$), and Tye-Gingras and Gosselin [31] had a MAE less than 0.01 respect to $k\Delta T/q_l$ (equivalent to MAE = 0.06 with respect to $\overline{\Theta}$). In this study, 0.02 was set as the threshold limits on the MAE and RMSD with respect to $\overline{\Theta}$.

RMSD was also used to compare the differences between $\overline{\Theta}$ obtained from other analytical solutions (i.e., the FLS solution and the MFLS solution) and $\overline{\Theta}$ from the FE COMSOL solution.

3.4. Criterion

In this study, one percent (1%) difference was employed as a criterion to decide whether the effects of buried depth are negligible. This criterion is consistent with the work of Molina-Giraldo et al. [30] who concluded that the influence of groundwater flow is not negligible if the groundwater flow has more than 1% influence on the results. In that situation, the borehole wall temperature variation (ΔT) must be calculated using MFLS model which considers groundwater flow, as opposed to using the standard FLS models

of Eskilson [17] and Zeng et al. [27] which do not take groundwater flow into consideration. Similarly, the effects of buried depth are not negligible when the discrepancy between the MFLSD solution and the MFLS solution is greater than 1% (i.e. $\left|\overline{\Theta_{MFLSD}} / \overline{\Theta_{MFLS}} - 1\right| > 1\%$). At that time, the *g*-function must be computed using the MFLSD solution instead of the MFLS solution to consider the effects of buried depth.

4. Single borehole

4.1. Verification of the MFLSD model

A comparison between the MFLSD solution and numerical solution was conducted. An example of the absolute difference between the MFLSD and numerical solutions for Pe = 0 and D = 2 m was displayed in Fig. 8. It was observed that the absolute difference is relatively huge (up to 1.88 °C) in short-term ($Fo < 3\times10^5$), and then it is stabilised and is kept under 0.06 °C in long-term ($Fo > 3\times10^5$). The larger absolute difference in short-term is caused by the line source assumption that neglect the geometry within the borehole. Therefore, the line source models are only valid in long-term simulations which is $Fo > 3\times10^5$ in this study.

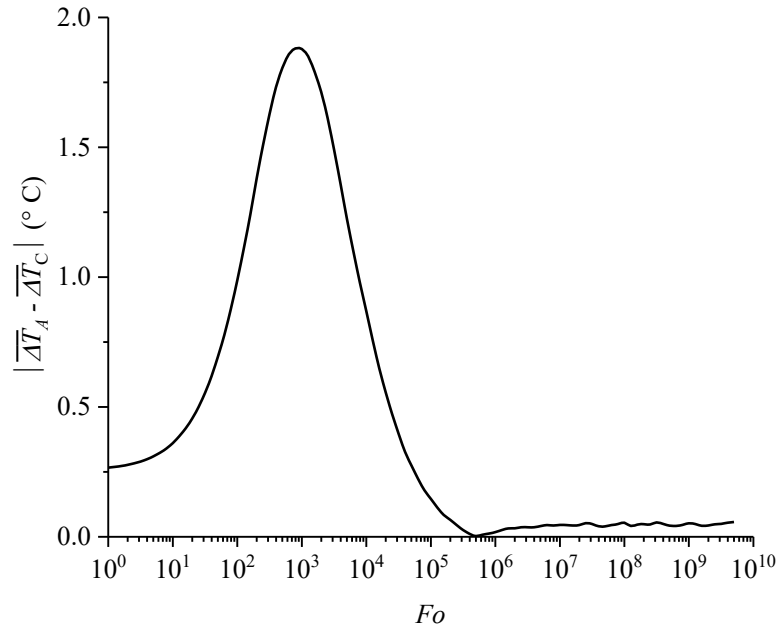

Figure 8. The absolute difference between the MFLSD and numerical solutions for Pe = 0 and D = 2 m.

As shown in Fig. 9, $\overline{\Delta T}$ was plotted against the Fourier number (Fo) for three buried depths (D = 0 m, D = 2 m and D = 8 m) and two Peclet numbers (Pe = 0 and Pe = 7.5). It is shown that the MFLSD solution exhibits a good agreement with the numerical solution generated with COMSOL Multiphysics over 100-year of continuous operation. As shown in Table 2, for the given parameters of this section, the MAE and RMSD yield values of about 0.007 and 0.007 respectively, which are lower than the thresholds of the acceptable MAE (0.02) and RMSD (0.02). Thus, the MFLSD solution was considered to be verified numerically.

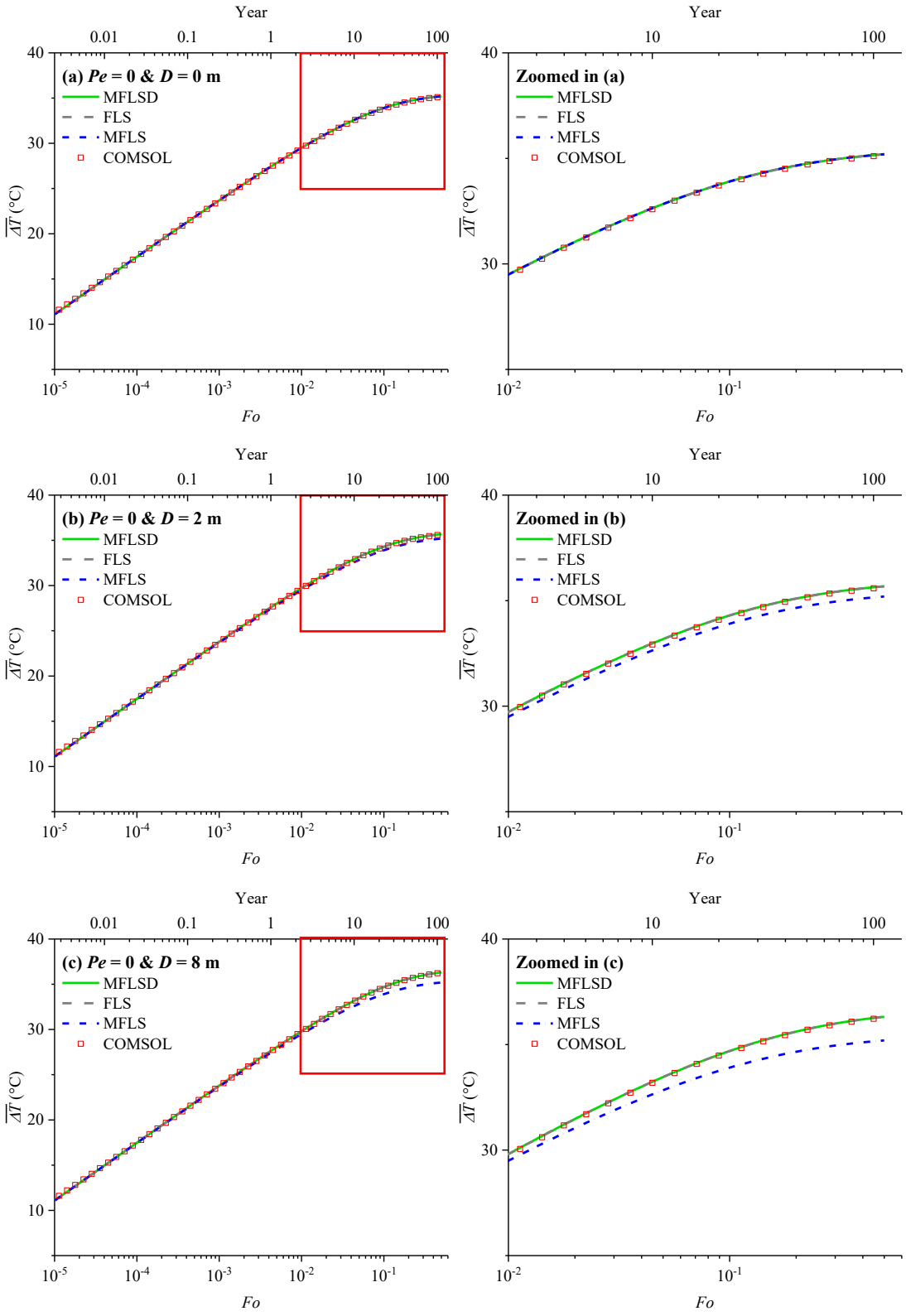
Year
0.01
0.1
1
10
100
(a) Pe = 0 & D = 0 m
MFLSD
FLS
MFLS
COMSOL
ΔT (°C)
Fo
Zoomed in (a)
(b) Pe = 0 & D = 2 m
Zoomed in (b)
(c) Pe = 0 & D = 8 m
Zoomed in (c)

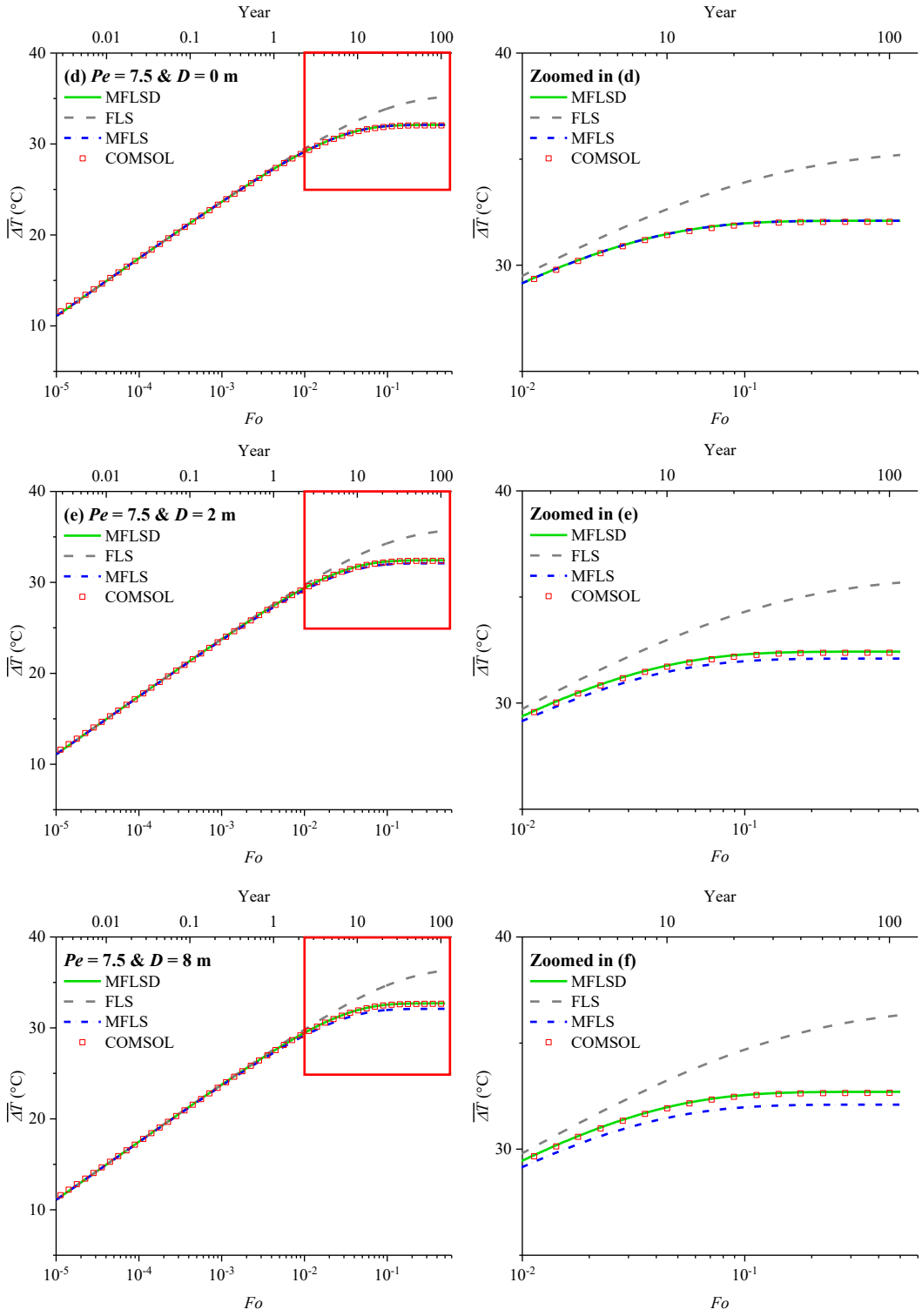

Figure 9. Borehole wall Temperature variations against Fourier number (*Fo*) for the given parameters (a) *Pe* = 0, *D* = 0 m; (b) *Pe* = 0, *D* = 2 m; (c) *Pe* = 0, *D* = 8 m; (d) *Pe* = 7.5, *D* = 0 m; (e) *Pe* = 7.5, *D* = 2 m; (f) *Pe* = 7.5, *D* = 8 m.

In addition, a comparison with the MFLS solution of Tye-Gingras and Gosselin [31] and the FLS solution of Claesson and Javed [29] was also carried out. Worth noting is that the MFLSD solution is identical with the MFLS solution for D = 0 m (Fig. 9a and 9d), and it is also identical with the FLS solution for Pe = 0 (Fig. 9a, 9b and 9c). For Pe = 7.5, the MFLSD and FLS solutions (Fig. 9d, 9e and 9f) start to differ by about 1% after two-year operation, and the dispersion grows as the simulation time increases. Compared with the FLS results, the temperature variations from the MFLSD solution is smaller, i.e. about 8.70%, 9.01%, and 9.82% for D = 0 m, 2 m, and 8 m at 100 years, respectively. These reductions can be explained by the effects of groundwater flow, through which accumulated heat at the borehole is broadly distributed [71]. For D = 8 m, results from the MFLSD solution are greater by about 3.15% and 1.88% for Pe = 0 and Pe = 7.5 at 100 years (Fig. 9c and 9f), respectively. Those differences indicate that neglecting buried depth can underestimate the temperature variation. The underestimation is caused by the thermal resistance of the ground layer between the ground surface and BHE. The thermal resistance diminishes the changes in temperature [39]. In general, both buried depth and groundwater flow influence the temperature variations in long-term. When incorporating the effects of buried depth and groundwater flow simultaneously (Fig. 9e and 9f), the MFLSD model provides a better prediction of the temperature variation. As shown in Table 2, MSRD always yields a smaller value for the MFLSD model.

Table 2. The MAE and MRSD between the non-dimensional temperature variations ($\overline{\Theta}$) predicted from analytical models and $\overline{\Theta}$ observed from the FE COMSOL model.

		Pe = 0			*Pe* = 7.5		
		D = 0 m (**a**)	2 m (**b**)	8 m (**c**)	*D* = 0 m (**d**)	2 m (**e**)	8 m (**f**)
MAE		0.007	0.007	0.007	0.007	0.007	0.007
RMSD	FLS	0.007	0.007	0.007	0.220	0.229	0.248
	MFLS	0.007	0.039	0.083	0.007	0.030	0.056
	MFLSD	0.007	0.007	0.007	0.007	0.008	0.007

4.2. Computational time

Computational time is another interesting aspect used to compare analytical solutions and numerical solutions. When a program is to be executed repeatedly, its computational time determines the productivity of the given program [72]. In this study, computational time represents the total amount of time required to execute MATLAB scripts or COMSOL simulations. In comparison, borehole wall temperature variations were computed using FLS solution [29], MFLS solution [31], MFLSD solution and 3D-FE COMSOL solution for *D* = 2 m and *Pe* = 7.5. Other borehole geometry and thermal properties are the same as those in the real case scenario.

The computational time of various time scale (i.e. hour, month, year and decade) simulations for each analytical and numerical solutions is shown in Table 3. Compared

with the FLS solution, the MFLSD solution is able to account for groundwater flow without any significant drawbacks on computational time. Meanwhile, using the method given by Claesson and Javed [29], the MFLSD solution reduces the computational time of the MFLS solution by approximately 16% in hourly and monthly simulation. In comparison with COMSOL solution, the MFLSD solution reduces the computational time by a factor of ten thousand times for monthly and yearly simulation. In addition, the COMSOL model failed to finish the hourly simulation due to the limited available disk space (5.4 TB). Thus, the MFLSD solution is more computationally efficient than a 3D numerical model from the viewpoint of time and space usage.

Table 3. Comparison of the computational time for the analytical solutions and numerical solutions.

		Computational time (s)			
Time scale	Number of points	COMSOL	FLS	MFLS	MFLSD
Hour	876000	N/A	382.62	471.80	397.01
Month	1200	6234	0.58	0.70	0.59
Year	100	3784	0.10	0.11	0.12
Decade	10	2992	0.06	0.06	0.07

4.3. Sensitivity study of the non-dimensional buried depth (d)

The MFLSD solution includes the effect of buried depth in the MFLS model. The MFLSD solution can be expressed as four variables in non-dimensional form, as shown in Eq. (33): $R_b = r_b / H$, $d = D / H$, Fourier number $Fo = \alpha t / H^2$ and Peclet number

$Pe = UH/\alpha$. To elucidate the role of buried depth, a sensitivity study was conducted based on the identified non-dimensional variables.

4.3.1 Effects of non-dimensional buried depth (*d*) on the temperature variation at various *Fo* values

Fig. 10 demonstrates the non-dimensional temperature variation $\overline{\Theta_{MFLSD}}(Fo)$ obtained with the MFLSD solution for $Pe = 0$ and $R_b = 0.001$. According to the typical length of a vertical borehole (50 m to 150 m) and selected values of buried depth (0 m to 8 m), a ratio of $d = D/H$ varying from 0 to 0.2 was considered for this study. Three other values (0.02, 0.05, and 0.1) were chosen within this range for the sensitivity study. In addition, a theoretical upper bound solution corresponding to $d = \infty$ was also tested [73] to set the upper limit of the solutions, although $d = \infty$ is unrealistic for practical applications. For every d value, $\overline{\Theta_{MFLSD}}(Fo)$ rises monotonically as Fo increases and eventually reaches a steady state. As shown in Table 4, as the ratio $d = D/H$ is enlarged from 0 to 0.2, the steady state value increases from 5.91 to 6.20. This increase can be explained by the thermal resistance of the ground layer above the BHE [39]. As the BHEs are buried further below the ground surface, the thermal resistance of the ground layer above the BHEs becomes larger, which reduces the heat flow between the BHEs and ground surface.

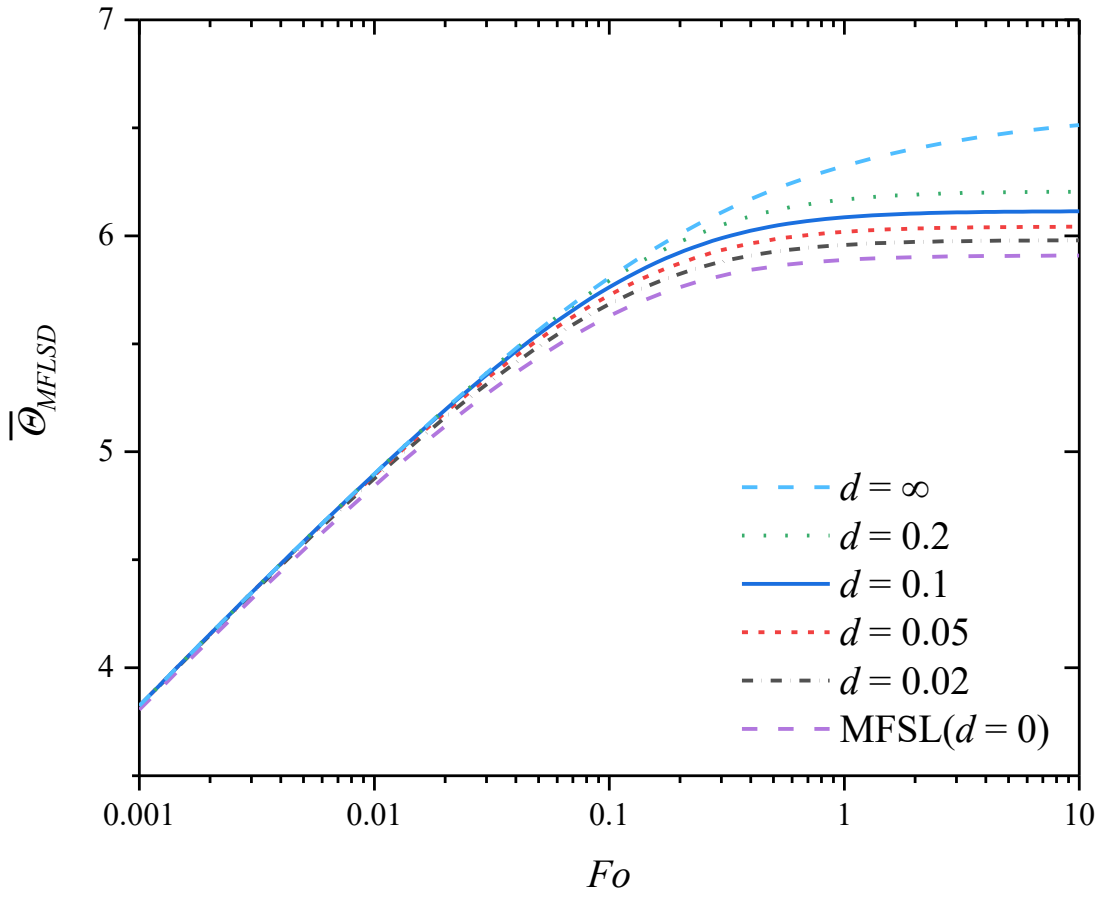

Figure 10. Non-dimensional temperature variations for Pe = 0 and R_b = 0.001 considering various non-dimensional buried depth (d) ranging from 0 to 0.2.

Also, it is shown in Fig. 10 that the influence of the buried depth becomes more evident for temperature variation in the long term. For example, at the beginning (Fo = *0.001*), the value of $\overline{\Theta_{MFLSD}}$ has virtually no difference; at a steady state, the value of $\overline{\Theta_{MFLSD}}$ rises by about 5.00% when the ratio $d = D/H$ varies from 0 to 0.2 (Table 4). According to the 1% criterion, the buried depth becomes negligible in the long term. In addition, the calculated value of $\overline{\Theta_{MFLSD}}$ is only for a single borehole in this chapter. For multiple

borehole configurations, the value of $\overline{\Theta_{MFLSD}}$ increases when there is a heat source interaction [73]. Therefore, it is concluded that the buried depth is a significant parameter that cannot be neglected in the generation of *g*-functions.

Table 4. Non-dimensional temperature variation for Pe = 0 and R_b = 0.001 considering various d ranging from 0 to 0.2.

	Non-dimensional temperature variation					
Fo	$d = 0$	0.02	0.05	0.1	0.2	∞
0.001	3.81	3.82	3.82	3.82	3.82	3.82
0.01	4.84	4.88	4.89	4.90	4.90	4.90
0.1	5.63	5.68	5.73	5.76	5.79	5.81
1	5.89	5.96	6.02	6.09	6.17	6.32
10	5.91	5.98	6.04	6.11	6.20	6.51

4.3.2 Effects of non-dimensional buried depth (*d*) on the temperature variation at various R_b values

The $\overline{\Theta_{MFLSD}}(R_b)$ was obtained with the MFLSD model for Pe = 0 considering various d ranging from 0 to 0.2 at the steady state. Boreholes are typically 0.1 m to 0.15 m in diameter [15]. According to the typical length of a vertical borehole (50 m to 150 m), a ratio of $R_b = r_b / H$ varying from 0.0003 to 0.0015 was considered. As shown in Fig. 11a,

the slopes of all the curves are similar. Therefore, the difference of two solutions ($\overline{\Theta_{MFLSD}} - \overline{\Theta_{MFLS}}$) was used to describe the discrepancy between the two solutions. Fig. 11b indicates that the difference between the two solutions is constant for any R_b values. The same phenomenon appears for any value of Fo in the considered range. In other words, the effects of buried depth are unaffected by the borehole radius.

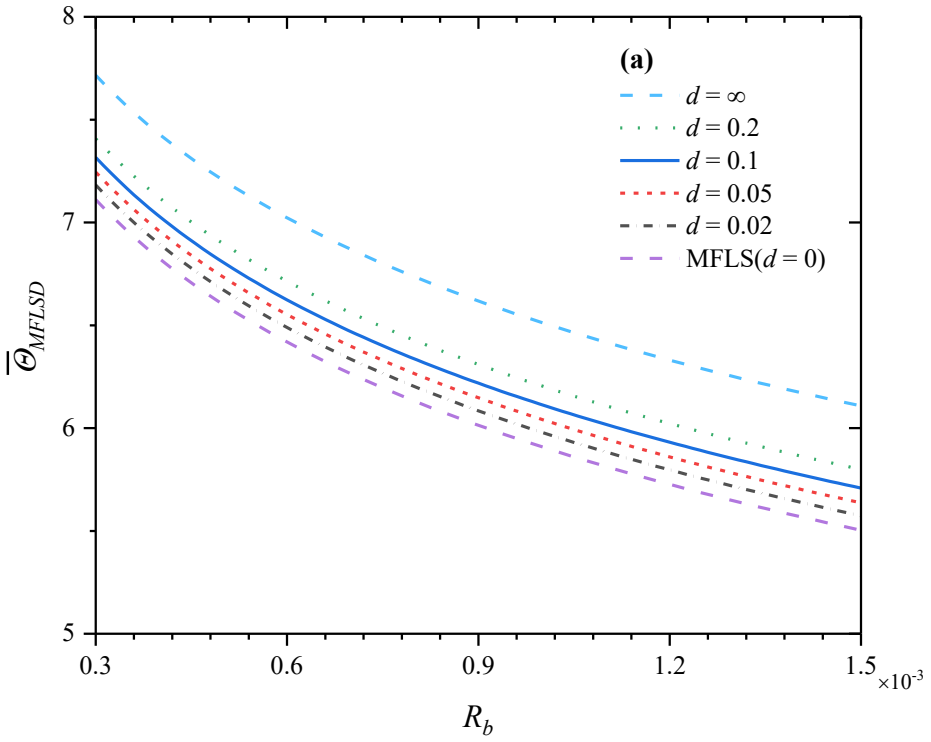

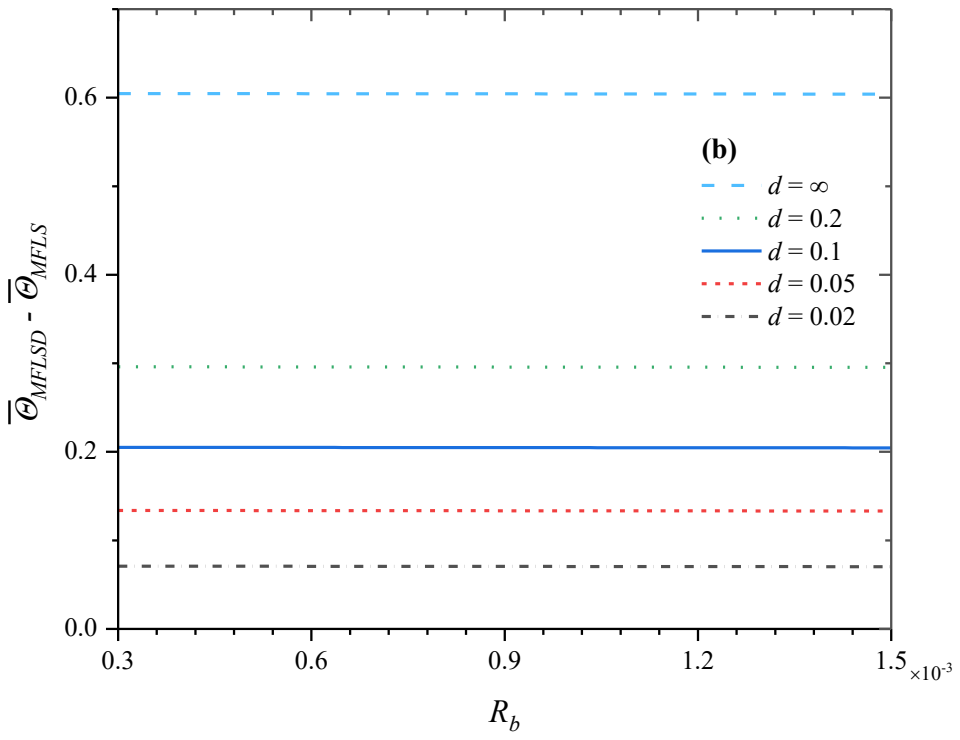

Figure 11. (a) Non-dimensional temperature variations for various non-dimensional buried depths (d) ranging from 0 to 0.2 and various non-dimensional borehole radii (R_b) ranging from 0.0003 to 0.0015 at a steady state (Fo = 10) and at Pe = 0. (b) The difference between the MFLS and MFLSD solutions for various d values.

4.3.3 Effects of non-dimensional buried depth (d) on the temperature variation at various Pe values

To evaluate the influences of both groundwater flow and buried depth, another comparison between the MFLSD solution ($\overline{\Theta_{MFLSD}}$) and the MFLS solution of Tye-Gingras and Gosselin ($\overline{\Theta_{MFLS}}$) was carried out. The ratio of $\overline{\Theta_{MFLSD}}/\overline{\Theta_{MFLS}}$ was used to describe the discrepancy between the two solutions. At the steady state, the percentage difference between two solutions for different buried depths and different Peclet numbers

$0.1 < Pe < 1000$ was plotted. Fig. 12 demonstrates that the increase of the groundwater flow velocity reduces the effect of buried depth. For example, for $d = 0.2$, the percentage of difference between the two solutions is about 5% for $Pe = 0.1$ and it falls to about 0.07% for $Pe = 1000$. Moreover, for $Pe > 100$, the curves at different buried depths are in close agreement with each other, which means the effect of groundwater advection eliminates the influence of buried depth. For $Pe > 22$, the discrepancy between the MFLS solution and the MFLSD solution for $d = \infty$ is less than 1%. Since the MFLSD solution for $d = \infty$ laid out the upper bound limit of the results [73], the percentage of difference between the two solutions for any buried depth are greater than 1% for $Pe < 22$. According to the one percent criterion, the g-function must be calculated by the MFLSD solution rather than by the MFLS solution for $Pe < 22$.

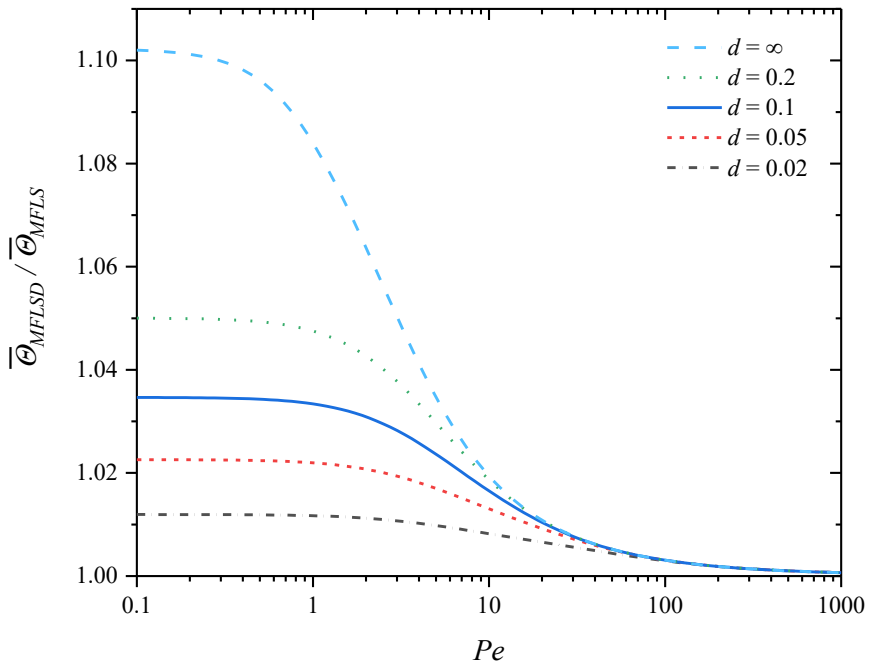

Figure 12. Percentage difference between the MFLS and MFLSD solutions for various non-dimensional buried depths (d) and various Peclet numbers (Pe).

4.4. Influence of buried depth at fixed borehole lengths

Although the aforementioned non-dimensional variables have obvious advantages, parameters with physical meanings including buried depth, borehole length and operation time are of great concern in engineering design. The MFLSD solution was simulated for common borehole lengths ranging from 50 m to 150 m and for Pe = 0. For each fixed borehole length, buried depth varied from 0 m to 8 m. Other borehole geometries and thermal properties were the same as in the real geoexchange system project. The simulation was run for 30 years which is the expected lifetime of GSHP systems [74]. The temperature variations were calculated using Eq. (31), and then the values were recast in non-dimensional forms.

By analyzing the $\overline{\Theta_{MFLSD}}$ against the time in years for Pe = 0 (as shown in Fig. 13), it can be demonstrated that the effect of buried depth increases as the borehole length decreases. For example, compared to the standard MFLS model (D = 0 m), the $\overline{\Theta_{MFLSD}}$ rises by 1.12% for a 150 m borehole that starts from 8 m below the surface and it rises by 3.55% if the borehole is only 50 m in length (see Table 5). The other Peclet number scenario (Pe = 7.5) was also calculated. Although the influence of groundwater flow reduces the effects of buried depth, $\overline{\Theta_{MFLSD}}$ still rises by 2.62% for a 50 m borehole for D = 8 m. According to the one percent criterion, the buried depth becomes an important parameter for the design of short BHEs. In contrast, Eskilson's original work [17] concluded that the exact value of buried depth is not important, since only small temperature variations (i.e., 0.1 °C) were found among several numerical simulations for buried depth of 2 m to 8 m with a fixed active borehole length H. Eskilson's [17] conclusion is adequate for

longer boreholes. As shown in Table 5, for a 150 m borehole, temperature variation increases by 0.58% when the buried depth varies from 2 m to 8 m. However, the conclusion is inadequate for a shallow borehole. For a 50 m borehole, the percentage difference is 1.83% between the temperature variations with D = 2 m and D = 8 m. Since the percentage difference is greater than 1%, these two cases need to be treated differently.

To summarize, in practical application, buried depth is a significant parameter in the design of short BHEs; the exact value of buried depth cannot be neglected.

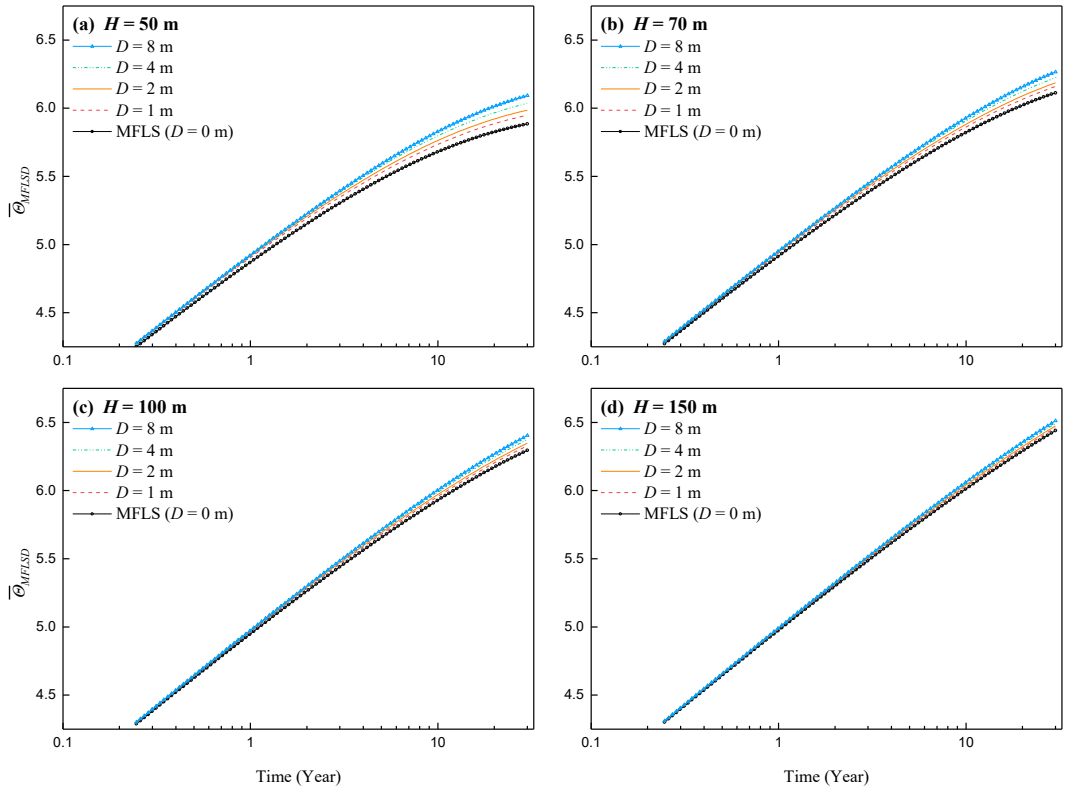

Figure 13. Non-dimensional temperature variations over time for Pe = 0 (a) H = 50 m, (b) H = 70 m, (c) H = 100 m, (d) H = 150 m.

Table 5. Non-dimensional temperature variations for different buried depths and groundwater flow scenarios at 30 years.

	Non-dimensional temperature variations				% Difference ($\overline{\Theta_{MFLSD}}/\overline{\Theta_{MFLS}}-1$)			
Pe = 0	H = 50 m	70 m	100 m	150 m	50 m	70 m	100 m	150 m
MFLS (D = 0 m)	**5.88**	**6.11**	**6.30**	**6.44**	**Ref**			
D = 1 m	5.95	6.16	6.33	6.46	1.08%	0.76%	0.52%	0.34%
2 m	5.99	6.19	6.35	6.47	1.72%	1.21%	0.83%	0.54%
4 m	6.04	6.22	6.37	6.49	2.57%	1.82%	1.24%	0.81%
8 m	6.09	6.27	6.40	6.51	3.55%	2.51%	1.72%	1.12%
Pe = 7.5	H = 50 m	70 m	100 m	150 m	50 m	70 m	100 m	150 m
MFLS (D = 0 m)	**5.57**	**5.72**	**5.83**	**5.92**	**Ref**			
D = 1 m	5.62	5.75	5.86	5.94	0.95%	0.66%	0.46%	0.30%
2 m	5.65	5.77	5.87	5.94	1.44%	1.01%	0.70%	0.46%
4 m	5.68	5.80	5.89	5.96	2.04%	1.43%	0.99%	0.65%
8 m	5.72	5.82	5.90	5.97	2.62%	1.84%	1.27%	0.83%

5. Multiple boreholes

In practical applications, multiple BHEs are common in large-scale commercial buildings that have high energy demands. The aforementioned MFLSD solution for a single borehole has provided a foundation for thermal analysis of a multiple borehole field. The MFLSD solution does not only determine the average temperature variation at the borehole wall, but also calculate the average temperature variation over the length of the borehole at any radial distance in any direction (Eq. (30)). In other words, the thermal interaction between two boreholes can be calculated using MFLSD solution for any distance (in any direction) separating the two boreholes in the multiple borehole field. For a multiple borehole field of 3 × 2 boreholes (described in Section 3.3), the distances are shown in Fig. 14. Then, the temperature variation of a specific borehole was calculated by linearly superposing all the temperature changes produced by individual BHE in the multiple BHE field. Using borehole 1 as an example, the non-dimensional temperature variation on the borehole 1 became

$$\begin{aligned}\overline{\Theta_1} = \overline{\Theta_{MFLS}}\left(R_b, Pe\right) + \overline{\Theta_{6\to1}}\left(\sqrt{5}B, cos^{-1}\left(\frac{-1}{\sqrt{5}}\right), -Pe\right) + \overline{\Theta_{5\to1}}\left(2B, 90°, Pe\right) \\ + \overline{\Theta_{4\to1}}\left(\sqrt{2}B, 135°, -Pe\right) + \overline{\Theta_{3\to1}}\left(B, 90°, Pe\right) + \overline{\Theta_{2\to1}}\left(B, 180°, -Pe\right)\end{aligned} \tag{39}$$

Finally, the *g*-function was obtained by averaging the non-dimentional temperature variation of all the boreholes in the multiple borehole field.

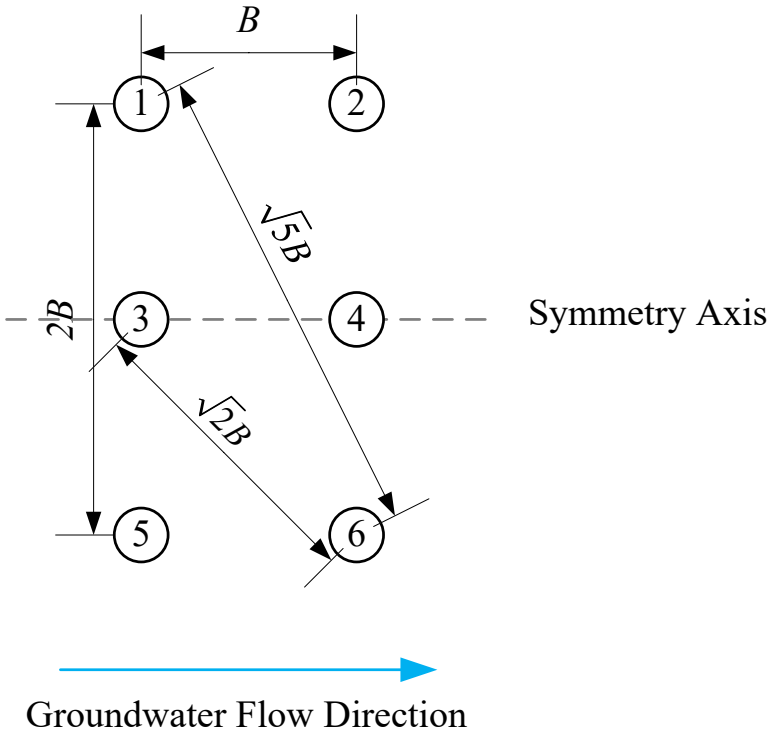

Figure 14. Distances in a multiple borehole field of 3 × 2 boreholes.

5.1. Numerical verification

Similar to the MFLSD solution for a single borehole, the *g*-functions for multiple borehole field is also verified numerically with a 3D-FE COMSOL model solving the same heat transfer problems. The COMSOL model of a single borehole in previous study is expanded to a multiple borehole field of 3 × 2 boreholes.

A preliminary analysis was done to ensure the simulation results are unaffected by the extension of the model domain and the size of elements. The procedure is similar to the one for single borehole. The preliminary analysis showed that the selected domain size for a single borehole is also valid for the multiple borehole field of 3 × 2 boreholes, since

the temperature changes at the external boundaries were less than 0.003 °C at the end of the simulations. The reliability of the domain size was also verified by comparing average temperature at the borehole wall. The mesh geometry with about eleven million (11,000,000) elements was selected to ensure the mesh independent.

The comparison between the analytical and numerical solution was conducted. As shown in Fig. 15, $\overline{\Delta T}$ in a borehole filed with 3 × 2 boreholes was plotted against Fourier number (Fo) for three borehole spacings (B = 6 m, B = 7.6 m and B = 8 m) and two Peclet numbers (Pe = 0 and Pe = 7.5). Moreover, $\overline{\Delta T}(Fo)$ with three different borehole configurations (1 × 2, 3 × 1 and 3 × 2) and two different buried depths (D = 2 m and D = 8 m) were displayed in Fig. 16. It is shown that the temperature variation obtained from g-function (using Eq. (1)) exhibits a good agreement with the numerical solution generated with COMSOL Multiphysics over 100-year (about Fo = 0.5) continuous operation. It can be seen from Table 6, for the given results of this section, the maximum values of MAE and RMSD are approximately 0.012 and 0.015 respectively, which are lower than the thresholds of the acceptable MAE (0.02) and RMSD (0.02). Therefore, the analytical g-functions for multiple boreholes were considered to be verified numerically.

Table 6. MAE and MRSD between the $\overline{\Theta}$ predicted from g-functions and $\overline{\Theta}$ observed from FE COMSOL model.

		RMSD	MAE
Pe = 0 D = 8 m 3 × 2 boreholes	B = 6 m	0.015	0.012
	7.6 m	0.013	0.010
	8 m	0.014	0.011
Pe = 7.5 D = 8 m 3 × 2 boreholes	B = 6 m	0.008	0.007
	7.6 m	0.007	0.006
	8 m	0.007	0.006
Pe = 7.5 B = 7.6 m 3 × 2 boreholes	D = 2 m	0.007	0.006
	8 m	0.007	0.006
Pe = 7.5 D = 2 m B = 7.6 m	3 × 2 boreholes	0.008	0.007
	3 × 1 boreholes	0.007	0.006
	1 × 2 boreholes	0.007	0.006

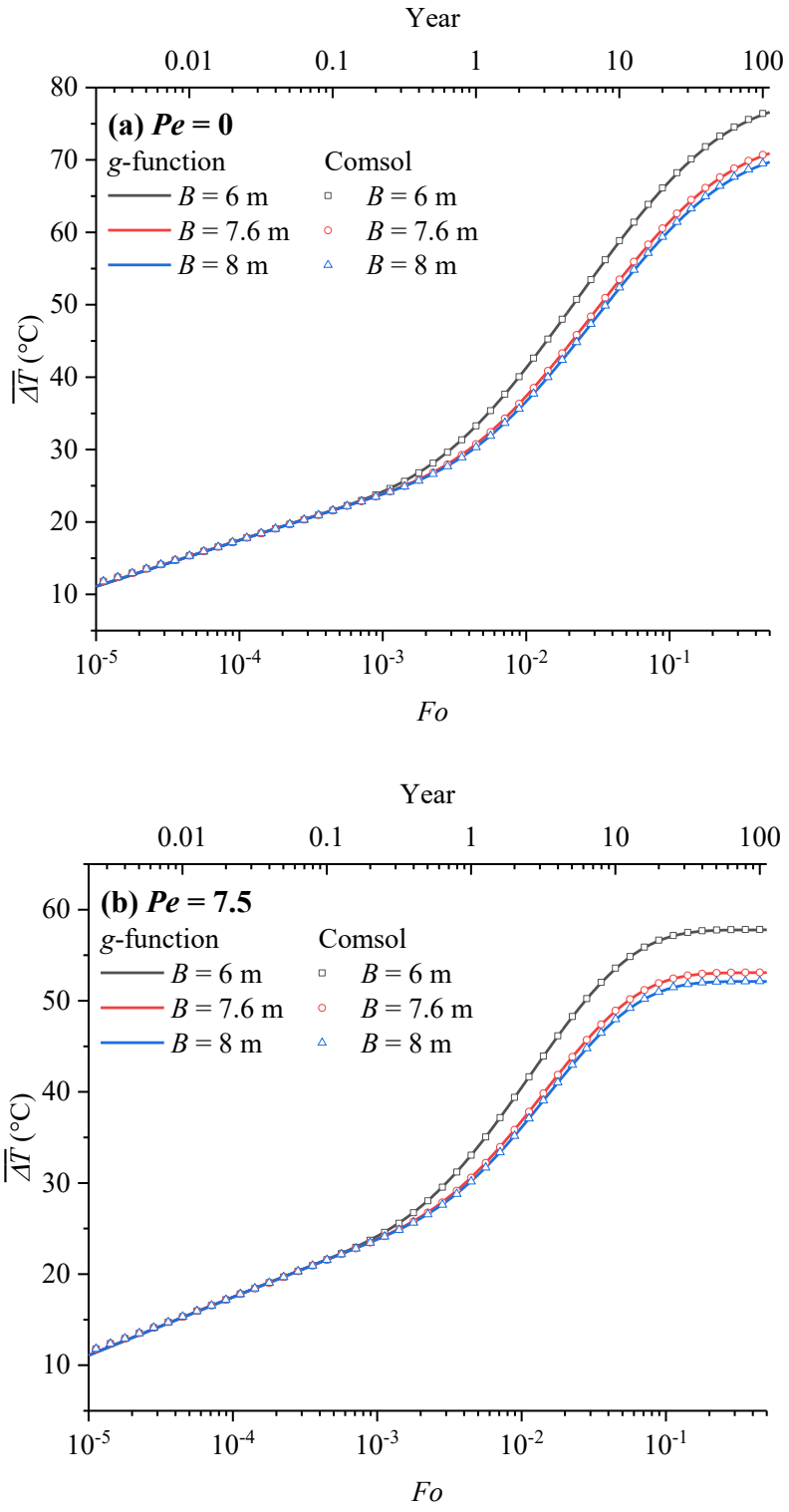

Figure 15. Borehole wall temperature variations in a borehole field with 3 × 2 boreholes against Fourier number (*Fo*) for the given parameters (a) *Pe* = 0 *D* = 8 m (b) *Pe* = 7.5 *D* = 8 m.

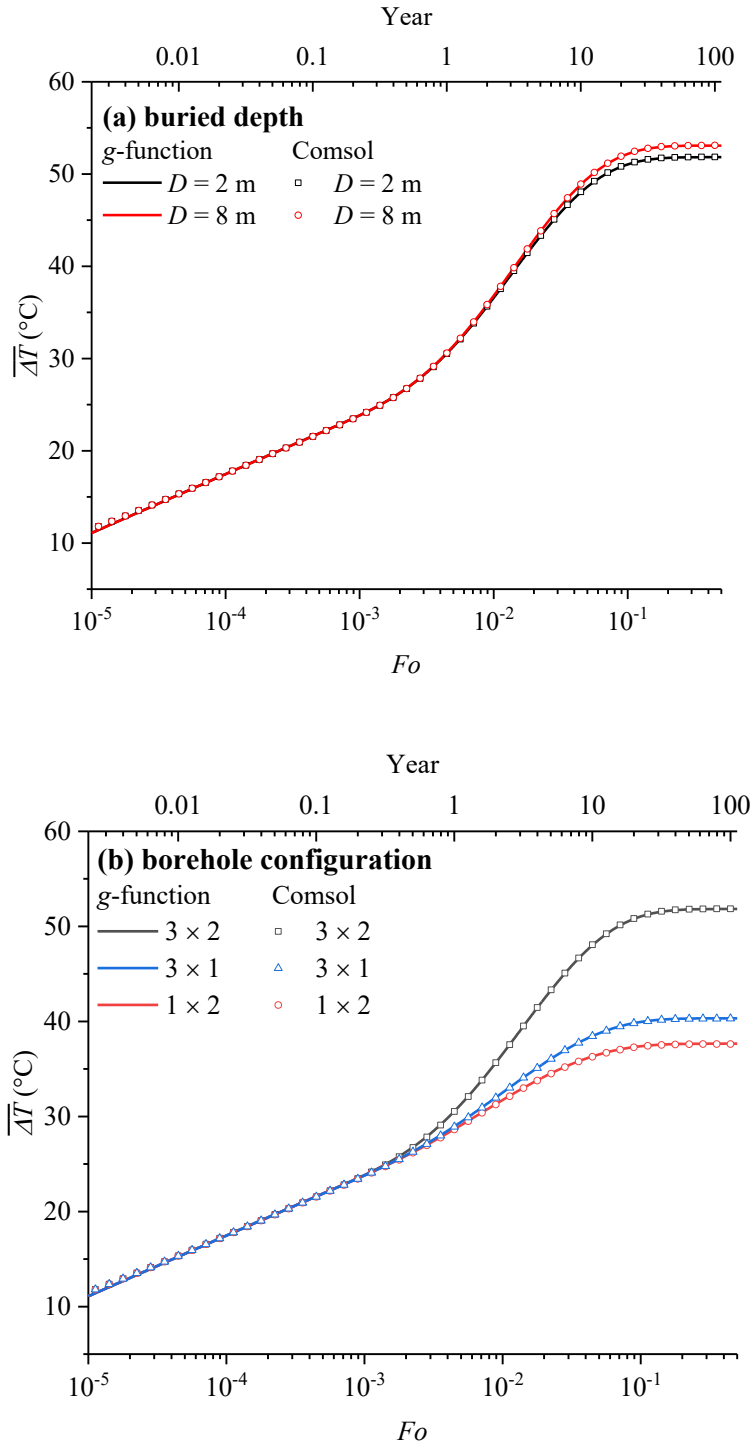

Figure 16. Borehole wall temperature variation against Fourier number (*Fo*) with three different borehole configurations (1 × 2, 3 × 1 and 3 × 2) and two different buried depths (D = 2 m and D = 8 m) for Pe = 7.5.

Computational time was also compared between the analytical solution and the numerical solution. The comparison indicated that using numerical model to determine temperature variation at the borehole wall is a time-consuming and computationally intensive task. For example, the COMSOL results shown in Fig. 15 and Fig. 16 were obtained from numerical simulations that calculated the temperature variation at 96 points in time. For a scenario with Pe = 7.5, D = 2 m and B = 7.6 m, the numerical simulation took 27,669 s (i.e., 7 hours 41 minutes 9 seconds) in computing. The other numerical simulations had a similar computational time at about 8 hours. On the contrary to the numerical simulation, the analytical simulation costed 0.94 s in the calculation of the 96 points in time, and it only took 3,813 s (i.e., 1 hours 03 minutes 33 seconds) in an hourly simulation which contains 876,000 points in time. Therefore, analytical *g*-functions are favored over numerical models for sizing, optimizing and simulating the BHE system due to their superior computational time.

5.2. Effects of thermal interaction

Analytical *g*-functions obtained from MFLSD model includes the effect of thermal interactions. To elucidate the role of thermal interaction in multiple borehole field, a sensitivity study was conducted based on the identified non-dimension variables. A simple rectangle configuration of 3 × 2 boreholes with an equal borehole spacing (B) was selected for the study.

5.2.1 Effects of thermal interaction on the temperature variation at various *Fo* values

Fig. 17 demonstrates the non-dimensional temperature variation $\overline{\Theta_{3\times2}}(Fo)$ obtained with the analytical *g*-functions for $Pe = 0, R_b = 0.001$, $d = 0.02$. Based on the ASHRAE's Handbook, the values of borehole spacing were chosen varying from 5 m to 8 m in this section. According to the typical length of a vertical borehole (50 m to 150 m), the ratio $b = B/H$ varying from 0.03 to 0.2 was considered. Two other values (0.06 and 0.1) were chosen within this range for the sensitivity study. In addition, a theoretical lower bound solution corresponding to $b = \infty$ was also tested to set the lower limit of the solutions, which is identical with the MFLSD solution for a single borehole. For every *d* value, $\overline{\Theta_{3\times2}}(Fo)$ rises monotonically as *Fo* increases and eventually reaches a steady state. As shown in Table 7, as the ratio $b = B/H$ reduces from 0.2 to 0.03, the steady state value increases from 9.62 to 17.64. This is because that the thermal interaction between distant boreholes becomes weaker [75]. For the same reason, the influence of the thermal interactions appears early with a shorter borehole spacing. For example, all the $\overline{\Theta_{3\times2}}(Fo)$ with different borehole spacing overlap at the beginning. Then, the $\overline{\Theta_{3\times2}}(Fo)$ for $b = 0.03$ is the first that increases dramatically than the others at $Fo > 10^{-4}$. In contrary, the $\overline{\Theta_{3\times2}}(Fo)$ for $b = 0.2$ has a similar sharp increase until $Fo > 4.5 \times 10^{-3}$. In general, the effect of the thermal interactions appears faster and is stronger when the B/H ration is smaller.

Table 7. Non-dimensional temperature variation for Pe = 0, R_b = 0.001 d = 0.02 considering various d ranging from 0 to 0.2.

	Non-dimensional temperature variation				
Fo	b = 0.03	0.06	0.1	0.2	∞
0.00003	2.10	2.10	2.10	2.10	2.10
0.0001	2.78	2.73	2.73	2.73	2.73
0.001	5.76	4.22	3.88	3.85	3.85
0.01	11.21	8.23	6.48	5.17	4.89
10	17.64	14.43	12.23	9.62	5.98

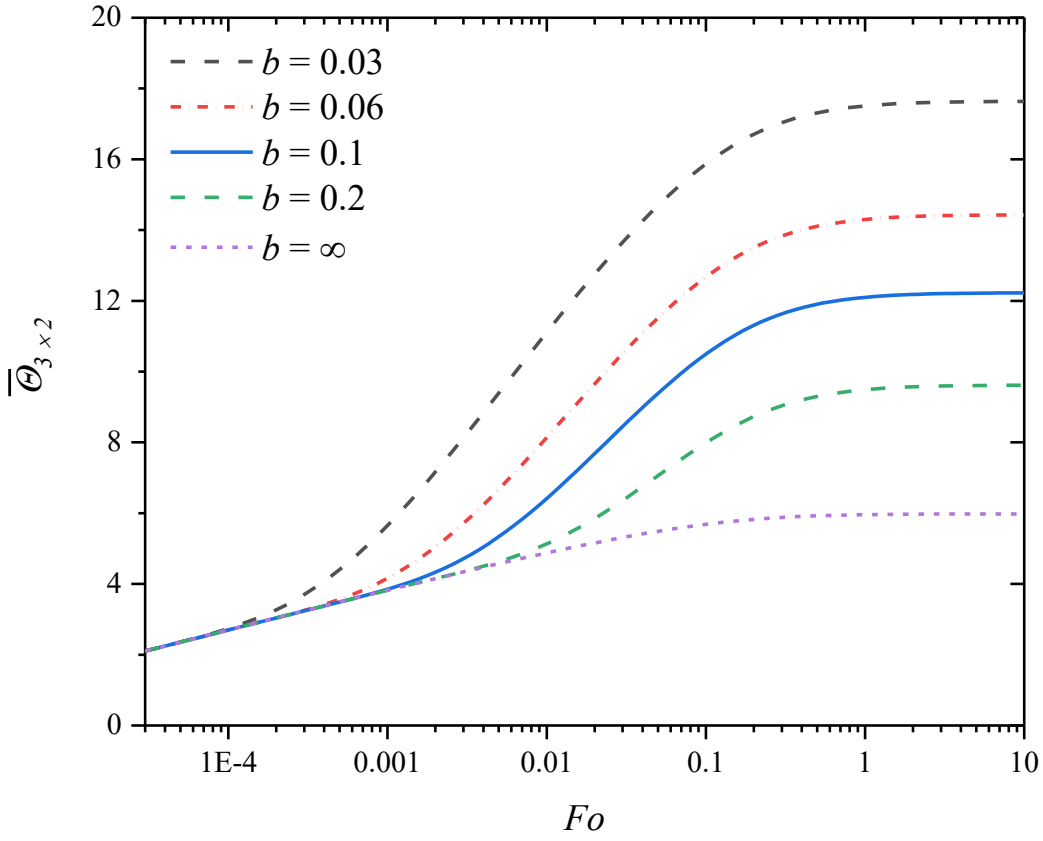

Figure 17. Non-dimensional temperature variations for $Pe = 0$, $R_b = 0.001$ and $d = 0.02$ considering various non-dimensional borehole spacings (b) ranging from 0 to 0.2.

5.2.2 Effects of buried depth (d) in multiple borehole field

To evaluate the influence of buried depth in multiple borehole field, a comparison between the MFLSD solution ($\overline{\Theta_{MFLSD}}$) for a single borehole and the g-function for multiple borehole was carried out. The effect of buried depth for a single borehole was already evaluated in Section 4.3. In this section, the effect of buried depth was evaluated for multiple boreholes.

Fig. 18 demonstrates the non-dimensional temperature variation $\overline{\Theta_{3\times2}}(Fo)$ obtained with b = 0.1. The other input parameters were set to be same as those used for the single borehole (Section 4.3.1). As shown in Fig. 18, $\overline{\Theta_{3\times2}}(Fo)$ rises as Fo increases and reaches a steady state eventually. As the ratio $d = D/H$ is enlarged from 0 to 0.2, the steady state limit increases by 12.22% (from 11.97 to 13.43). The percentage difference is much lager then the one (5.00%) obtained from $\overline{\Theta_{MFLSD}}$ for a single borehole (Section 4.3.1). It is an expected behaviour since the thermal interaction between the boreholes were linearly added up. Therefore, it is concluded that the buried depth is a significant parameter that cannot be neglected in the design of BHEs system.

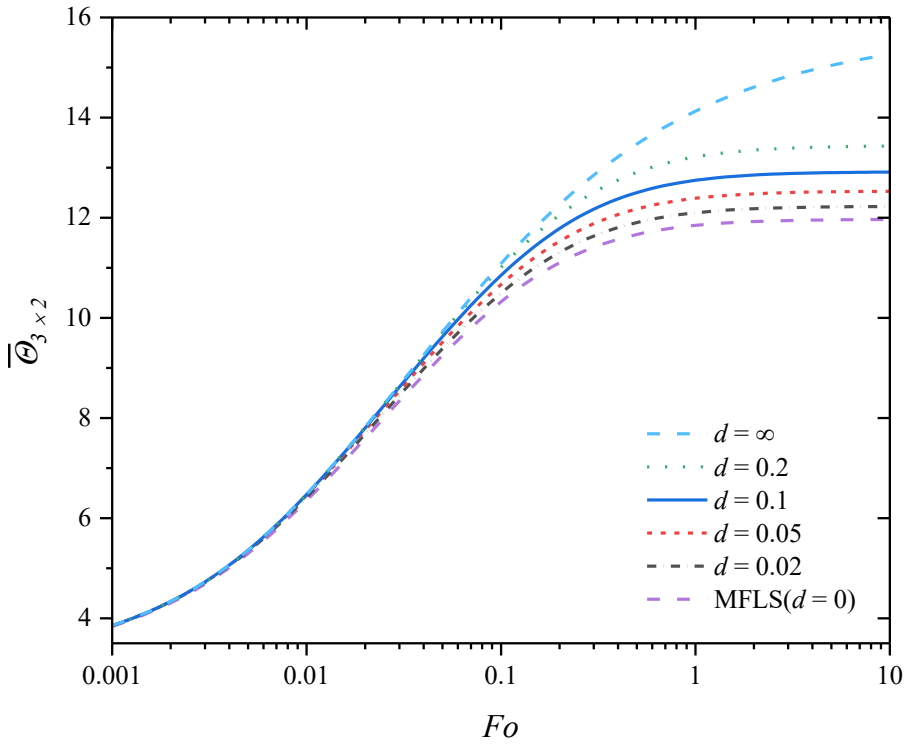

Figure 18. Non-dimensional temperature variations for Pe = 0, R_b = 0.001 and b = 0.1 considering various non-dimensional buried depths (d) ranging from 0 to 0.2.

5.3. Influence of buried depth at fixed borehole lengths

As aforementioned in Section 4.4, parameters with physical meanings are of great concern in the engineering design, including the borehole length, buried depth and operation time. The non-dimensional borehole wall temperature variation was calculated for a common borehole length ranging from 50 m to 150 m, Pe = 0 and B = 7.6 m with various buried depths from 0 m to 8 m. Other borehole geometries and thermal properties were the same as those in the real geoexchange system project. The simulation was run for 30 years which is the expected lifetime of GSHP systems [74].

The $\overline{\Theta_{3\times2}}$ against the time in years has a similar pattern with $\overline{\Theta_{MFLSD}}$. As shown in Fig. 19, it is demonstrated that the impact of buried depth grows as the borehole length drops. For example, with regard to the standard MFLS model (D = 0 m), the $\overline{\Theta_{MFLSD}}$ rises by 2.39% for a 150 m borehole buried 8 m below the surface and it rises by 8.49% if the borehole is only 50 m in length (see Table 8). Compering with the result obtained in Section 4.4, the rising in $\overline{\Theta}$ is much larger for multiple borehole field than for a single borehole. For example, when H = 70 m, the temperature variation for a single borehole increases by 0.83% when the buried depth varies from 0 m to 2 m (see Table 5); in the multiple borehole field, the temperature variation increases by 1.48% when the buried depth varies from 0 m to 2 m. According to the one percent criterion, buried depth becomes an important parameter for the design of BHEs in practical application.

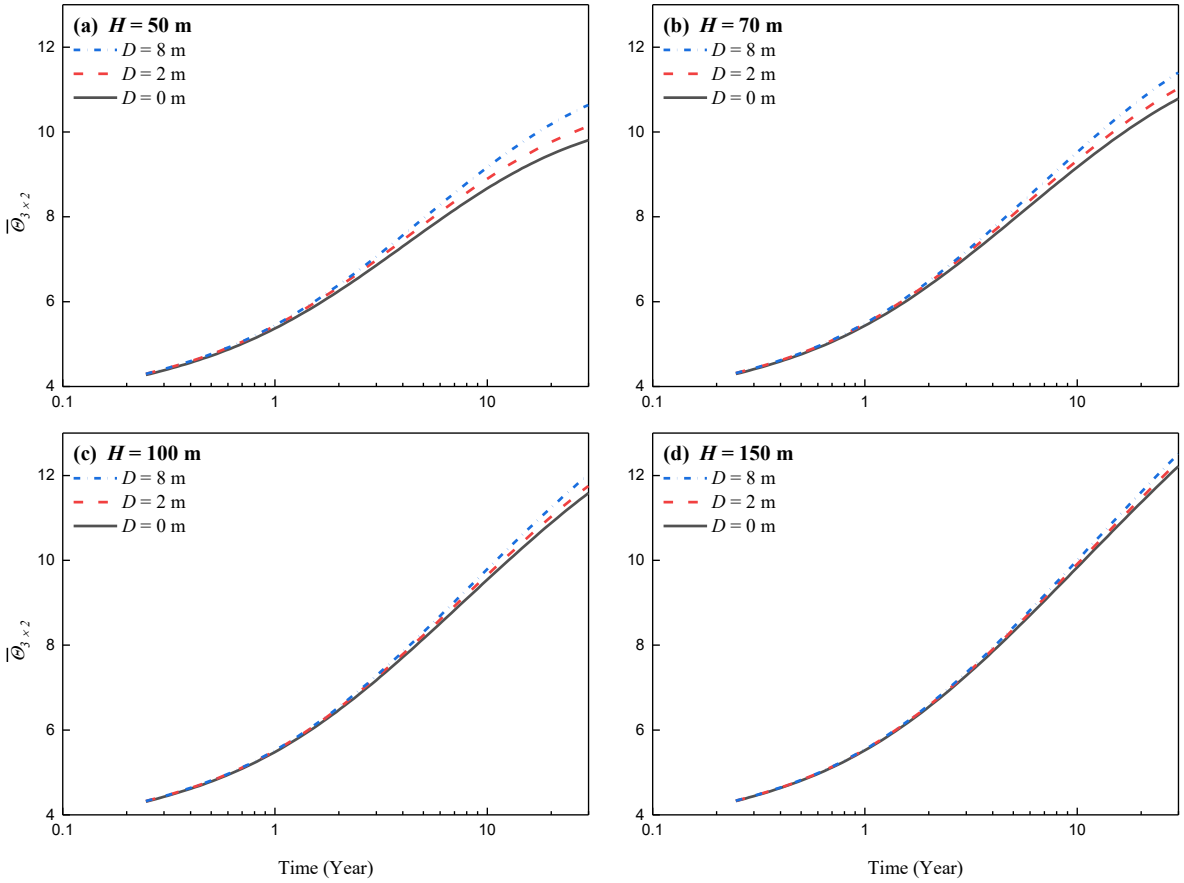

Figure 19. Temperature variations over time for $Pe = 0$ and $B = 7.6$ m (a) $H = 50$ m; (b) $H = 70$ m; (c) $H = 100$ m; (d) $H = 150$ m.

Table 8. Non-dimensional temperature variation for different buried depths and groundwater flow scenarios at 30 years.

	Non-dimensional temperature variations				% Difference			
	H = 50 m	70 m	100 m	150 m	50 m	70 m	100 m	150 m
D = 0 m	9.81	10.79	11.59	12.22	**Ref**			
2 m	10.13	11.03	11.76	12.33	3.32%	2.25%	1.48%	0.93%
8 m	10.64	11.41	12.02	12.51	8.47%	5.75%	3.78%	2.39%

6. Conclusion

The following conclusions were drawn from the study:

(1) A new single integral solution of the moving finite line source (MFLS) model was generated to consider the effect of buried depth. The new solution (MFLSD) gives the average temperature variation over the borehole surface at any borehole radius. The MFLSD solution is verified numerically with a three-dimensional (3D) finite-element (FE) COMSOL model. Compared with the 3D-FE COMSOL model, the MFLSD solution is more computationally efficient from the viewpoint of time and space usage.

(2) In general, both groundwater flow and buried depth have certain effects on the temperature variation of a borehole heat exchanger (BHE) in a long-time simulation. The effect of buried depth diminishes heat transfer between the ground surface and BHE; and the effect of groundwater flow balances the accumulated heat in the ground gradually. The MFLSD solution, incorporating the effects of buried depth and groundwater flow at the same time, provides a more accurate estimation of the *g*-functions, leading to a more thermal-effective design.

(3) The effect of buried depth heavily depends on the groundwater velocity. The increase of the groundwater flow velocity reduces the effect of buried depth. In a very high groundwater flow velocity scenario (i.e., $Pe > 100$), the effect of groundwater advection eliminates the influence of buried depth. For $Pe < 22$, the MFLSD solution must be used over the standard MFLS model to consider the

combined effects of buried depth and groundwater flow when calculating temperature variation.

(4) The effect of buried depth becomes larger with regard to long-term temperature variation as the borehole length reduces. For the given parameters in this study, for a long borehole (H = 150 m), the average non-dimensional temperature rises by about 1.12% as the buried depth increase from 0 m to 8 m; for a short borehole (H = 50 m), the non-dimensional temperature rises by about 3.55% with the same change in buried depth. In practical application, buried depth is a significant parameter in the design of short BHEs; the exact value of buried depth cannot be neglected.

(5) The MFLSD solution was combined with a spatial superposition procedure to compute the *g*-functions for the borehole field. The *g*-functions are also verified numerically with a three-dimensional (3D) finite-element (FE) COMSOL model.

(6) The effect of buried depth is more significant in a borehole field containing multiple boreholes due to the accumulation effects of the buried borehole. For the given parameters in this study, for a single borehole with H = 100 m, the average non-dimensional temperature rises by about 0.83% as the buried depth increase from 0 m to 2 m; in a multiple borehole field with 3 × 2 boreholes, the non-dimensional temperature rises by about 1.48% with the same change in buried depth. Therefore, the buried depth becomes an important parameter in the design of BHEs.

7. Limitations and future work

(1) The development of the MFLSD solution is based on the homogeneous ground assumption: the ground is assumed to be uniform along the vertical depth of a borehole. In practical applications, the boreholes are normally drilled through different layers, and these layers have different thermal properties and the hydro-geological conditions. Particularly, water table (the upper surface of the zone of the saturated ground) is generally found at a certain depth underneath the ground surface, and the water table fluctuates seasonally and from year to year [76]. Therefore, the homogeneous assumption can lead to unreliable results [41]. To avoid the associated limitation of homogeneous ground assumption, multiple ground layers will be taken account into the MFLSD solution in the future study.

(2) The development of line source model assumes that a constant heat flux is applied along the borehole length, i.e. constant heat flux boundary condition, and the temperature on the borehole wall changes accordingly. On the other hand, another boundary condition, uniform temperature boundary condition, is also commonly used for generating *g*-functions [77-79]. The uniform temperature boundary condition assumes that a uniform temperature is applied along the borehole length and all boreholes have the same temperature at the borehole wall [78]. Note that Eskilson's *g*-functions were computed using the uniform temperature boundary condition [17]. An dispersion between the Eskilson's *g*-functions and the analytical *g*-functions, which obtained from the FLS model with the constant heat flux boundary condition, was observed [28, 77, 78, 80]. The dispersion is greater for larger borehole fields [78]. For example, Monzo et al. [77] found that the

difference between the results with the two different boundary conditions are virtually insignificant for a small multiple borehole field of 2 × 3 boreholes, and Cimmino and Bernier [78] found that the differences become 52% at the steady state for a large multiple borehole field of 10 × 10 boreholes. However, there is no work has been done to determine which boundary condition has a better agreement with the practical condition. Therefore, future study will be devoted to evaluating the differences between the practical condition and the two assumed boundary conditions.

References

[1] S.A. Ghoreishi-Madiseh, A.P. Sasmito, F.P. Hassani, L. Amiri, Performance evaluation of large scale rock-pit seasonal thermal energy storage for application in underground mine ventilation, Applied Energy, 185 (2017) 1940-1947.

[2] J.N.d.l. Vergne, Hard Rock Miner's Handbook, 5 ed., Stantec Consulting, Edmonton, Alberta, Canada, 2014.

[3] C. Keating, Harvesting heat from mine water, in: CIM Magazine, Canada Insititute of Mining, Westmount, QC, Canada, 2016.

[4] J. Menéndez, A. Ordónez, J.M. Fernández-Oro, J. Loredo, M.B. Díaz-Aguado, Feasibility analysis of using mine water from abandoned coal mines in Spain for heating and cooling of buildings, Renewable Energy, 146 (2020) 1166-1176.

[5] G.R. Watzlaf, T.E. Ackman, Underground mine water for heating and cooling using geothermal heat pump systems, Mine water and the environment, 25 (1) (2006) 1-14.

[6] J.W. Lund, T.L. Boyd, Direct utilization of geothermal energy 2015 worldwide review, Geothermics, 60 (2016) 66-93.

[7] M.H. Ahmadi, M.A. Ahmadi, M.S. Sadaghiani, M. Ghazvini, S. Shahriar, M.A. Nazari, Ground source heat pump carbon emissions and ground-source heat pump systems for heating and cooling of buildings: A review, Environmental Progress & Sustainable Energy, (2017).

[8] G. Florides, S. Kalogirou, Ground heat exchangers—A review of systems, models and applications, Renewable energy, 32 (15) (2007) 2461-2478.

[9] F. Cheruy, J.L. Dufresne, S. Aït Mesbah, J.Y. Grandpeix, F. Wang, Role of Soil Thermal Inertia in Surface Temperature and Soil Moisture-Temperature Feedback, Journal of Advances in Modeling Earth Systems, 9 (8) (2017) 2906-2919.

[10] S. Grasby, D. Allen, S. Bell, Z. Chen, G. Ferguson, A. Jessop, M. Kelman, M. Ko, J. Majorowicz, M. Moore, Geothermal energy resource potential of Canada. Geological Survey of Canada,. Open File 6914, in, 2011.

[11] I. Sarbu, C. Sebarchievici, General review of ground-source heat pump systems for heating and cooling of buildings, Energy and Buildings, 70 (2014) 441-454.

[12] U. Lucia, M. Simonetti, G. Chiesa, G. Grisolia, Ground-source pump system for heating and cooling: Review and thermodynamic approach, Renewable and Sustainable Energy Reviews, 70 (2017) 867-874.

[13] J. Luo, J. Rohn, M. Bayer, A. Priess, Thermal efficiency comparison of borehole heat exchangers with different drillhole diameters, Energies, 6 (8) (2013) 4187-4206.

[14] M.A. Bernier, Closed-loop ground-coupled heat pump systems, Ashrae Journal, 48 (9) (2006) 12.

[15] ASHRAE, 34 Geothermal energy, in: 2015 ASHRAE Handbook - Heating, Ventilating, and Air-Conditioning Applications (SI Edition), American Society of Heating, Refrigerating and Air-Conditioning Engineers, Inc., 2015.

[16] S. Miglani, K. Orehounig, J. Carmeliet, A methodology to calculate long-term shallow geothermal energy potential for an urban neighbourhood, Energy and Buildings, 159 (2018) 462-473.

[17] P. Eskilson, Thermal analysis of heat extraction boreholes, (1987).

[18] H. Yang, P. Cui, Z. Fang, Vertical-borehole ground-coupled heat pumps: A review of models and systems, Applied Energy, 87 (1) (2010) 16-27.

[19] M. Li, A.C.K. Lai, Review of analytical models for heat transfer by vertical ground heat exchangers (GHEs): A perspective of time and space scales, Applied Energy, 151 (Supplement C) (2015) 178-191.

[20] A. Priarone, M. Fossa, Modelling the ground volume for numerically generating single borehole heat exchanger response factors according to the cylindrical source approach, Geothermics, 58 (2015) 32-38.

[21] J.D. Spitler, GLHEPRO-A design tool for commercial building ground loop heat exchangers, in: Proceedings of the fourth international heat pumps in cold climates conference, Citeseer, 2000.

[22] G. Hellström, B. Sanner, Earth energy designer, User's Manual, version, 2 (2000).

[23] D. Bauer, W. Heidemann, H.J.G. Diersch, Transient 3D analysis of borehole heat exchanger modeling, Geothermics, 40 (4) (2011) 250-260.

[24] P. Monzó, A.R. Puttige, J. Acuña, P. Mogensen, A. Cazorla, J. Rodriguez, C. Montagud, F. Cerdeira, Numerical modeling of ground thermal response with borehole heat exchangers connected in parallel, Energy and Buildings, 172 (2018) 371-384.

[25] C. Yavuzturk, J.D. Spitler, S.J. Rees, A transient two-dimensional finite volume model for the simulation of vertical U-tube ground heat exchangers, ASHRAE transactions, 105 (2) (1999) 465-474.

[26] P. Monzó, Comparison of different Line Source Model approaches for analysis of Thermal Response Test in a U-pipe Borehole heat Exchanger, in, 2011.

[27] H.Y. Zeng, N.R. Diao, Z.H. Fang, A finite line-source model for boreholes in geothermal heat exchangers, Heat Transfer—Asian Research, 31 (7) (2002) 558-567.

[28] L. Lamarche, B. Beauchamp, A new contribution to the finite line-source model for geothermal boreholes, Energy and Buildings, 39 (2) (2007) 188-198.

[29] J. Claesson, S. Javed, An analytical method to calculate borehole fluid temperatures for time-scales from minutes to decades, in: ASHRAE Transactions, 2011, pp. 279-288.

[30] N. Molina-Giraldo, P. Blum, K. Zhu, P. Bayer, Z. Fang, A moving finite line source model to simulate borehole heat exchangers with groundwater advection, International Journal of Thermal Sciences, 50 (12) (2011) 2506-2513.

[31] M. Tye-Gingras, L. Gosselin, Generic ground response functions for ground exchangers in the presence of groundwater flow, Renewable Energy, 72 (2014) 354-366.

[32] T.V. Bandos, Á. Montero, E. Fernández, J.L.G. Santander, J.M. Isidro, J. Pérez, P.J.F.d. Córdoba, J.F. Urchueguía, Finite line-source model for borehole heat exchangers: effect of vertical temperature variations, Geothermics, 38 (2) (2009) 263-270.

[33] M. Cimmino, B.R. Baliga, A hybrid numerical-semi-analytical method for computer simulations of groundwater flow and heat transfer in geothermal borehole fields, International Journal of Thermal Sciences, 142 (2019) 366-378.

[34] M. Samson, J. Dallaire, L. Gosselin, Influence of groundwater flow on cost minimization of ground coupled heat pump systems, Geothermics, 73 (2018) 100-110.

[35] A. Capozza, M. De Carli, A. Zarrella, Investigations on the influence of aquifers on the ground temperature in ground-source heat pump operation, Applied Energy, 107 (2013) 350-363.

[36] J. Hecht-Méndez, M. de Paly, M. Beck, P. Bayer, Optimization of energy extraction for vertical closed-loop geothermal systems considering groundwater flow, Energy Conversion and Management, 66 (2013) 1-10.

[37] M. de Paly, J. Hecht-Méndez, M. Beck, P. Blum, A. Zell, P. Bayer, Optimization of energy extraction for closed shallow geothermal systems using linear programming, Geothermics, 43 (2012) 57-65.

[38] J. Hu, An improved analytical model for vertical borehole ground heat exchanger with multiple-layer substrates and groundwater flow, Applied Energy, 202 (Supplement C) (2017) 537-549.

[39] M. Cimmino, M. Bernier, F. Adams, A contribution towards the determination of g-functions using the finite line source, Applied Thermal Engineering, 51 (1-2) (2013) 401-412.

[40] J.A. Rivera, P. Blum, P. Bayer, Influence of spatially variable ground heat flux on closed-loop geothermal systems: Line source model with nonhomogeneous Cauchy-type top boundary conditions, Applied Energy, 180 (2016) 572-585.

[41] S. Erol, B. François, Multilayer analytical model for vertical ground heat exchanger with groundwater flow, Geothermics, 71 (Supplement C) (2018) 294-305.

[42] J.D. Spitler, M. Bernier, 2 - Vertical borehole ground heat exchanger design methods, in: S.J. Rees (Ed.) Advances in Ground-Source Heat Pump Systems, Woodhead Publishing, 2016, pp. 29-61.

[43] P. Eslami-nejad, M. Bernier, Freezing of geothermal borehole surroundings: A numerical and experimental assessment with applications, Applied Energy, 98 (2012) 333-345.

[44] G. Dalla Santa, Z. Farina, H. Anbergen, W. Rühaak, A. Galgaro, Relevance of computing freeze-thaw effects for borehole heat exchanger modelling: A comparative case study, Geothermics, 79 (2019) 164-175.

[45] S.o.M.a.A.E.-O.S. University, GLHEPro 4.1 For Windows Users' Guide, in, International Ground Source Heat Pump Association, 2014.

[46] N.R. Diao, Q.Y. Li, Z.H. Fang, Heat transfer in ground heat exchangers with groundwater advection, International Journal of Thermal Sciences, 43 (12) (2004) 1203-1211.

[47] S. Gehlin, Thermal response test: method development and evaluation, Luleå tekniska universitet, 2002.

[48] A.D. Chiasson, S.J. Rees, J.D. Spitler, A preliminary assessment of the effects of groundwater flow on closed-loop ground source heat pump systems, in, Oklahoma State Univ., Stillwater, OK (US), 2000.

[49] H. Fujii, R. Itoi, J. Fujii, Y. Uchida, Optimizing the design of large-scale ground-coupled heat pump systems using groundwater and heat transport modeling, Geothermics, 34 (3) (2005) 347-364.

[50] H. Wang, C. Qi, H. Du, J. Gu, Thermal performance of borehole heat exchanger under groundwater flow: A case study from Baoding, Energy and Buildings, 41 (12) (2009) 1368-1373.

[51] M. Fossa, A fast method for evaluating the performance of complex arrangements of borehole heat exchangers, HVAC&R Research, 17 (6) (2011) 948-958.

[52] L. Ingersioll, O.J. Zobel, A.C. Ingersoll, Heat Conduction: With Engineering Geological And Other Applications, Oxford And Ibh Publishing Co.; Calcutta; Bombay; New Delhi, 1954.

[53] G. Geothermal, Ground Loop Design™ Premier 2016 User's Guide, in, USA, 2016.

[54] H. Carslaw, J. Jaeger, Heat in solids, Clarendon Press, Oxford, 1959.

[55] D. Marcotte, P. Pasquier, F. Sheriff, M. Bernier, The importance of axial effects for borehole design of geothermal heat-pump systems, Renewable Energy, 35 (4) (2010) 763-770.

[56] J.H. Lienhard, A heat transfer textbook, Courier Corporation, 2013.

[57] T.V. Bandos, Á. Montero, P. Fernández de Córdoba, J.F. Urchueguía, Improving parameter estimates obtained from thermal response tests: Effect of ambient air temperature variations, Geothermics, 40 (2) (2011) 136-143.

[58] M.G. Sutton, D.W. Nutter, R.J. Couvillion, A Ground Resistance for Vertical Bore Heat Exchangers With Groundwater Flow, Journal of Energy Resources Technology, 125 (3) (2003) 183-189.

[59] R.J. Grosh, E.A. Trabant, G.A. Hawkins, Temperature distribution in solids of variable thermal properties heated by moving heat sources, Quarterly of Applied Mathematics, 13 (2) (1955) 161-167.

[60] D.G. Duffy, Green's functions with applications, Chapman and Hall/CRC, 2015.

[61] T. Metzger, Dispersion thermique en milieux poreux: caractérisation expérimentale par technique inverse, Institut National Polytechnique de Lorraine, 2002.

[62] J.A. Rivera, P. Blum, P. Bayer, A finite line source model with Cauchy-type top boundary conditions for simulating near surface effects on borehole heat exchangers, Energy, 98 (2016) 50-63.

[63] D. Marcotte, P. Pasquier, Fast fluid and ground temperature computation for geothermal ground-loop heat exchanger systems, Geothermics, 37 (6) (2008) 651-665.

[64] T. Katsura, K. Nagano, S. Narita, S. Takeda, Y. Nakamura, A. Okamoto, Calculation algorithm of the temperatures for pipe arrangement of multiple ground heat exchangers, Applied Thermal Engineering, 29 (5) (2009) 906-919.

[65] A. Faghri, Y. Zhang, 4 - Generalized governing equations for multiphase systems: averaging formulations, in: A. Faghri, Y. Zhang (Eds.) Transport Phenomena in Multiphase Systems, Academic Press, Boston, 2006, pp. 238-330.

[66] X. Zhang, W. Liu, Z. Liu, Criterion for local thermal equilibrium in forced convection flow through porous media, Journal of Porous Media, 12 (11) (2009) 1103-1111.

[67] J. Komar, Thermal conductivity test report, in, rEvolve Engineering Inc., 2014.

[68] C. Naldi, E. Zanchini, A new numerical method to determine isothermal g-functions of borehole heat exchanger fields, Geothermics, 77 (2019) 278-287.

[69] R. Perez, T.E. Hoff, Chapter 10 - SolarAnywhere Forecasting, in: J. Kleissl (Ed.) Solar Energy Forecasting and Resource Assessment, Academic Press, Boston, 2013, pp. 233-265.

[70] C. Zhang, Z. Guo, Y. Liu, X. Cong, D. Peng, A review on thermal response test of ground-coupled heat pump systems, Renewable and Sustainable Energy Reviews, 40 (2014) 851-867.

[71] E. Zanchini, S. Lazzari, A. Priarone, Long-term performance of large borehole heat exchanger fields with unbalanced seasonal loads and groundwater flow, Energy, 38 (1) (2012) 66-77.

[72] A.V. Aho, J.D. Ullman, Foundations of computer science, Computer Science Press, 1995.

[73] T.V. Bandos, Á. Campos-Celador, L.M. López-González, J.M. Sala-Lizarraga, Finite cylinder-source model for energy pile heat exchangers: Effect of buried depth and heat load cyclic variations, Applied Thermal Engineering, 96 (2016) 130-136.

[74] B. Huang, V. Mauerhofer, Life cycle sustainability assessment of ground source heat pump in Shanghai, China, Journal of Cleaner Production, 119 (2016) 207-214.

[75] A. Gultekin, M. Aydin, A. Sisman, Effects of arrangement geometry and number of boreholes on thermal interaction coefficient of multi-borehole heat exchangers, Applied Energy, 237 (2019) 163-170.

[76] W.M. Alley, T.E. Reilly, O.L. Franke, Sustainability of ground-water resources, US Department of the Interior, US Geological Survey, 1999.

[77] P. Monzó, P. Mogensen, J. Acuña, F. Ruiz-Calvo, C. Montagud, A novel numerical approach for imposing a temperature boundary condition at the borehole wall in borehole fields, Geothermics, 56 (2015) 35-44.

[78] M. Cimmino, M. Bernier, A semi-analytical method to generate g-functions for geothermal bore fields, International Journal of Heat and Mass Transfer, 70 (2014) 641-650.

[79] L. Lamarche, g-function generation using a piecewise-linear profile applied to ground heat exchangers, International Journal of Heat and Mass Transfer, 115 (2017) 354-360.

[80] M. Fossa, The temperature penalty approach to the design of borehole heat exchangers for heat pump applications, Energy and Buildings, 43 (6) (2011) 1473-1479.

[81] J.A. Rivera, P. Blum, P. Bayer, Analytical simulation of groundwater flow and land surface effects on thermal plumes of borehole heat exchangers, Applied Energy, 146 (Supplement C) (2015) 421-433.

Appendices

A. Comparison study of analytical models

A comprehensive review of the analytical line source models for a single borehole was presented in Ch.2. To illustrate the difference between these analytical models, a comparison study was carried out. Using the same input parameters (Section 3.2), the temperature variations at the borehole wall were calculated by the mathematical solutions of these four analytical models: the ILS solution (Eq. (5)) by Carslaw and Jaeger [54], the FLS solution (Eq. (12)) by Bandos et al. [32], the MILS solution (Eq. (16)) by Diao et al. [46], and MFLS solution (Eq. (21)) by Rivera et al. [62]. then the values were recast in non-dimensional form.

Before the comparison study, the velocity of the groundwater flow needs to be presumed since the hydraulic condition was not tested in the project. Molina-Giraldo et al. [30] found that the difference between MILS model and MFLS model is greater than 1% for $Pe < 10$, and the difference between FLS model and MFLS model is greater than 1% for $Pe > 1.2$. Based on these findings, Molina-Giraldo et al. concluded that the use of MFLS model is necessary for a Pe ranging between 1.2 to 10 [20, 30]. The same one percent criterion was adapted for this study. To define a suitable Pe value for illustrating the difference between these analytical models, the ratio of $\overline{\Theta_{MFLS}}/\overline{\Theta_{MILS}}$ and the ratio of $\overline{\Theta_{MFLS}}/\overline{\Theta_{FLS}}$ the were calculated for 1,000-year operation. Fig. A1. shows that the MFLS solution differs from the MILS solution by more than 1% for $Pe < 80.76$ and differs from the FLS solution by more than 1% for $Pe > 1.87$. It is indicated that the MFLS model is distinguishable from the other models for a Pe ranging between 1.87 to 80.76 in our case.

Therefore, a uniform Darcy velocity at $u_d = 4\times10^{-8}$ ms^{-1} corresponding to Pe = 7.5 was used in the study.

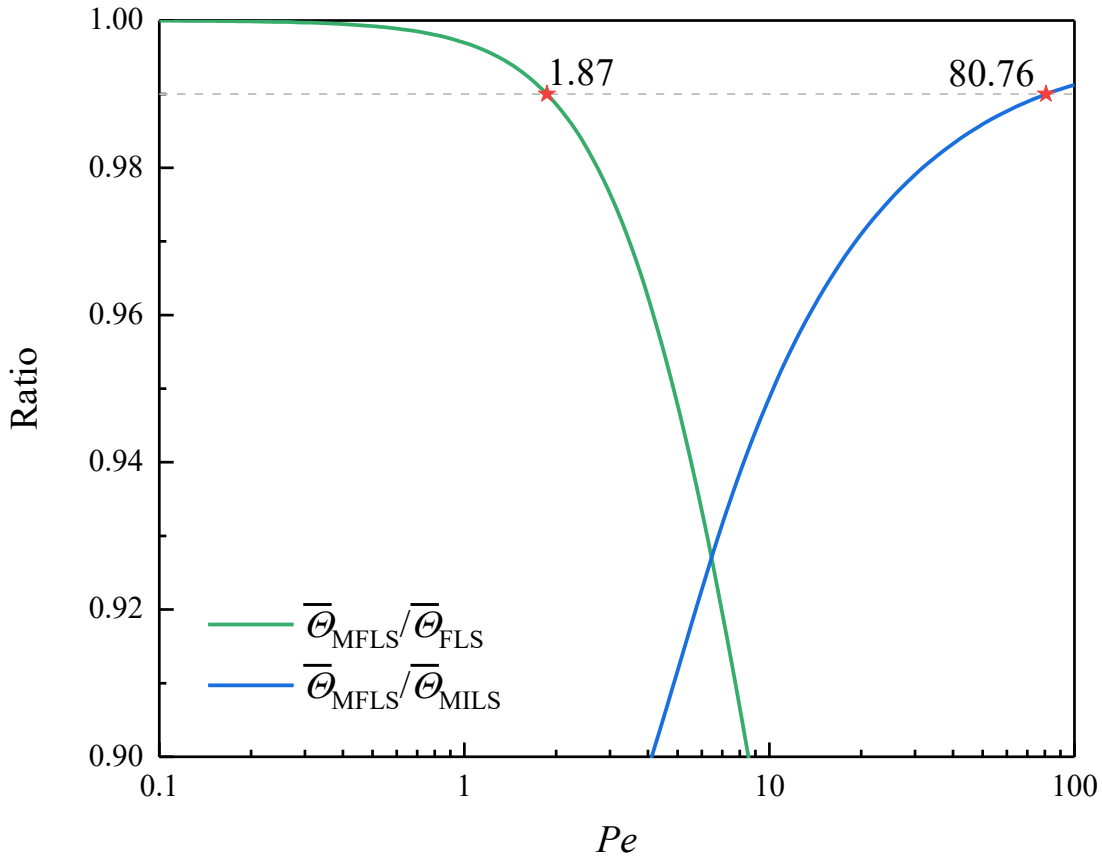

Figure A1. Ratio of $\overline{\Theta_{MFLS}}/\overline{\Theta_{MILS}}$ and the ratio of $\overline{\Theta_{MFLS}}/\overline{\Theta_{FLS}}$.

Once the velocity of the groundwater flow is defined, the temperature variations at the borehole wall can be calculated by the mathematical solutions of analytical models. As shown in Fig. A2 and Table A1, all temperature responses increase with time, and they are in close agreement with each other in the first month. In particularly, in the first 50 hours (a typical duration of TRT test), the results of the ILS solution and the other solutions (FLS, MILS and MFLS) differ by about 0.32%. This small difference indicates that, in short-term, the other models cannot provide much more information regarding the

influence of axial heat conduction and groundwater flow. After the first month, the temperature variations from the ILS and MFLS solutions started to be more different (i.e., $\overline{\Theta_{MFLS}}/\overline{\Theta_{ILS}} \approx 99\%$), and the dispersion increases as the simulation time increases. The dispersion between the ILS solution and the FLS solution becomes noticeable (i.e., $\overline{\Theta_{FLS}}/\overline{\Theta_{ILS}} < 99\%$) after 48 days. This dispersion can be explained by the effect of axial heat conduction, which accelerates the heat exchange at the bottom of the borehole and transfers the imbalance heat of extraction and injection on a year-round basis to the ambient air through the ground surface [27, 30]. As a result of the axial effect, the ILS solution yields the non-dimensional temperature of 8.48 without convergence and the FLS solution reaches steady-state value of 6.33 after one thousand years. The dispersion between the ILS and MILS solutions and it between the FLS and MFLS solutions become noticeable (i.e., $\overline{\Theta_{MILS}}/\overline{\Theta_{ILS}} < 99\%$, $\overline{\Theta_{MFLS}}/\overline{\Theta_{FLS}} < 99\%$) after 1.73 years and 1.90 years respectively. These dispersions can be explained by the synergistic effect of groundwater flow, by which the accumulated heat is balanced [46]. This effect becomes more evident if the Darcy velocity increases [30]. After one thousand years, and the MILS and MFLS model obtain the non-dimensional temperature variations to steady-state values of 6.12 and 5.73 respectively. Note that thirty-year is the expected lifetime of GSHP systems [74]. After thirty years continuous operation, the ratio of $\overline{\Theta_{MFLS}}/\overline{\Theta_{FLS}}$ and the ratio of $\overline{\Theta_{MFLS}}/\overline{\Theta_{MILS}}$ both are about 94%. The 6% difference indicates that neglecting groundwater flow or axial heat conduction can cause an overestimation of ground temperature variation. This ultimately results in an underestimation of geothermal

potential, leading to an over-conservative borehole design and increasing the unnecessary cost [81].

Table A1. Non-dimensional integrated mean borehole wall temperature variation with various specified time period obtained from four various analytical solutions.

Durations	1 hour	1 day	1 month	1 year	30 years	1000 years
ILS	0.59	2.08	3.78	5.03	6.73	8.48
FLS	0.59	2.08	3.75	4.92	6.11	6.33
MILS	0.59	2.08	3.78	5.00	6.09	6.12
MFLS	0.59	2.08	3.74	4.89	5.72	5.73

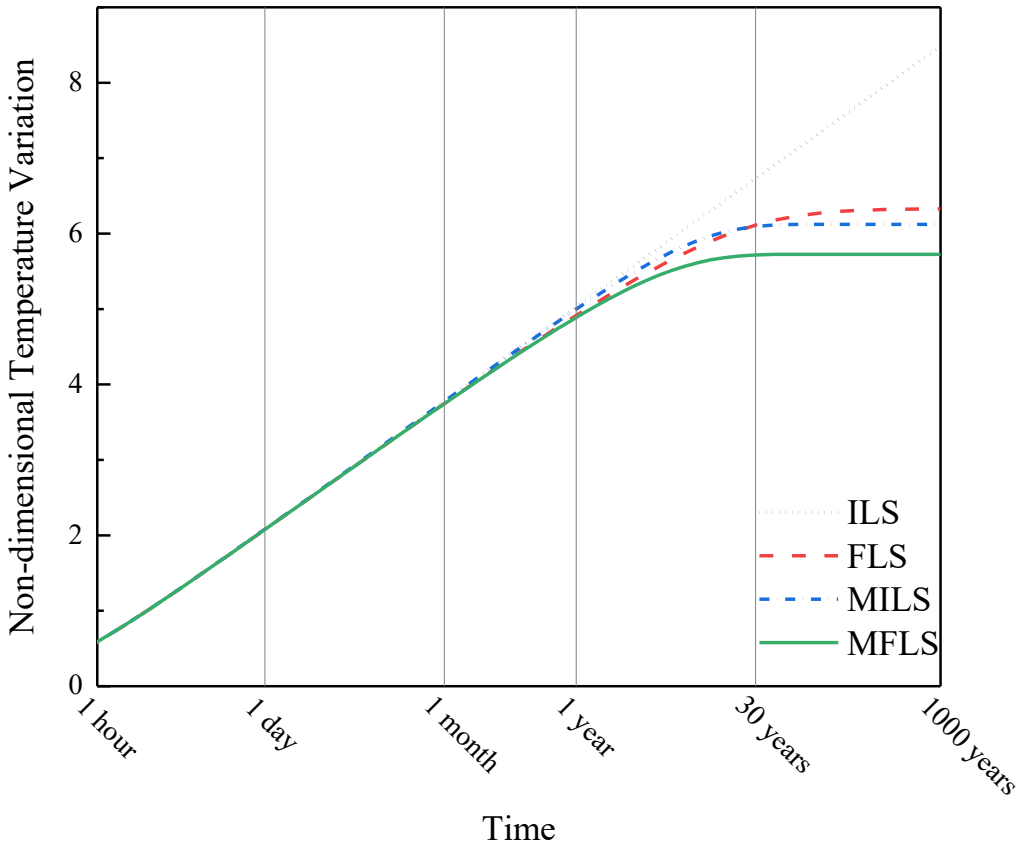

Figure A2. Comparison of various analytical models for non-dimensional temperature variations (A log-10 scale of time is used in the *x*-axis).

B. Model domain and mesh selection

A preliminary analysis has been done to ensure the simulation results are independent from the model domain and the mesh geometry. Referring to the work of Molina-Giraldo et al. [30], the domain dimension was enlarged starting from a horizontal domain size of (x = 200 m) × (y = 50 m) with a thickness of (z = 130 m), till the maximum temperature changes at the external boundaries are less than 0.005 °C at the end of the simulations. In principle, the temperature at far boundary supposed to be kept in undisturbed condition; the selected 0.005 °C tolerance assures a reasonable domain size and preserve the calculation accuracy [20].

The maximum temperature changes at the external boundaries are tabulated in Table B1 for each domain size. The domain extensions were firstly determined in a purely heat conduction scenario (Pe = 0) with a buried depth of 8 m. After that, a uniform groundwater flow was assigned throughout the entire domain aligned with x-axis. Due to the influence of groundwater flow, the model domain was further extended in positive x-direction. Finally, the 3D-FE model was constructed with a domain size of (x = 800 m) × (y = 200 m) × (z = 320 m). The same domain size is also valid for a multiple borehole field of3 × 2 boreholes. Worth noticing, the reliability of the domain size was also verified by comparing average temperature at borehole wall, which has relative differences less than 1% in the last extension.

Table B1. The maximum temperature changes at the external boundaries.

	Single borehole				Multiple boreholes
Negative *x*-direction and *y*-direction	50 m	100 m	150 m	200 m	200 m
Maximum temperature (°C)	3.0468	0.3736	0.0436	0.0036	0.0028
z-direction	130 m	180 m	230 m	280 m	280 m
Maximum temperature (°C)	1.1026	0.1487	0.0149	0.0010	0.0009
Positive *x*-direction	200 m	400 m	600 m		600 m
Maximum temperature (°C)	0.5243	0.0096	0.0002		0.0003

About the mesh, extremely fine elements were chosen near the borehole, and coarser elements were chosen at further locations to reduce mesh numbers (see Fig. B1). Tye-Gingras and Gosselin [31] suggested that a mesh-independent solution can be obtained when doubling the number of meshes yielded a relevant difference of less than 1% on the results for every time-step. Therefore, a comparison of average borehole wall temperature was carried out with an increasing number of elements on the borehole wall boundary. In our case, when the number of elements of the domain doubled from about one million to two million, the maximum difference on the average borehole wall temperature is about 0.04% (between 35.52 °C and 35.65 °C) in the considered time domain. This difference is acceptable since it is far less than 1%. Finally, the mesh geometry with about two

million (2,000,000) elements was selected which assure a reasonable number of elements and preserve the calculation accuracy.

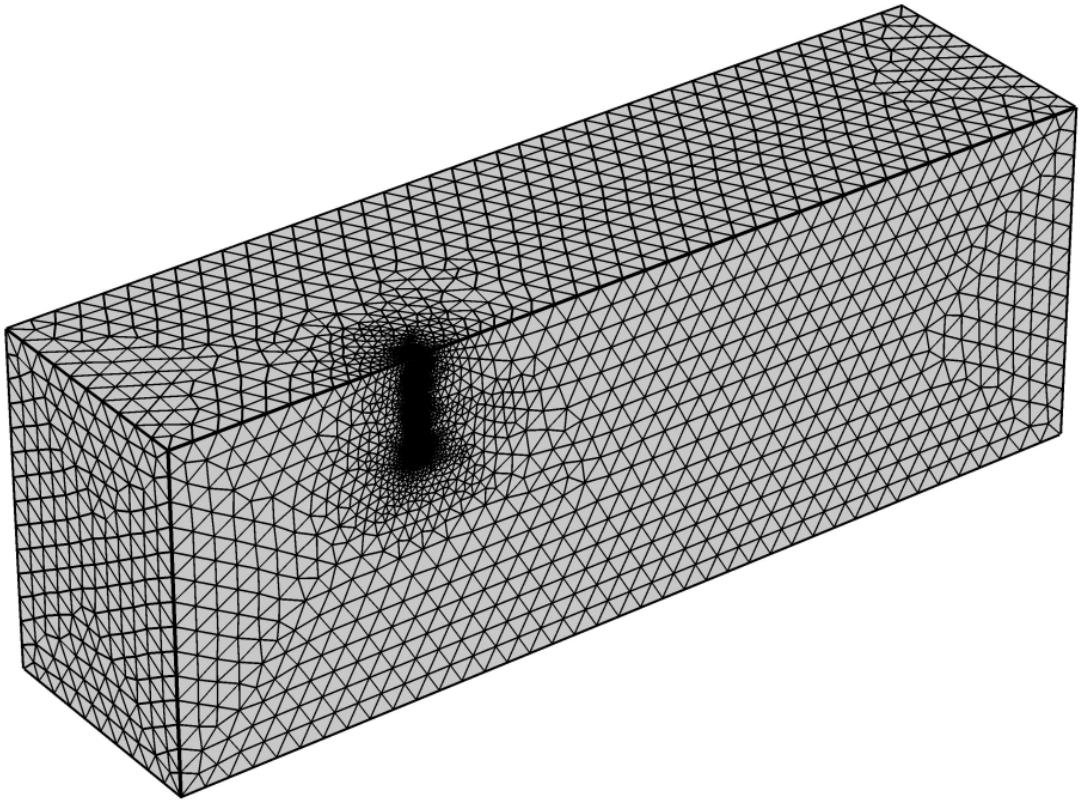

Figure B1. Mesh used in numerical simulations.

C. Isotherms obtained from the MFLSD model

The MFLSD solution provides the average temperature variation over the length of the borehole at any radial distance in any direction (Eq. (30)). In order to have a better understanding of the effects of buried depth, isotherms for a single borehole with various buried depth was plotted. The isotherms delineate the average temperature variation over the borehole length (H = 70 m) for Pe = 7.5 after 30-year operation. As shown in Fig. C1, the buried depth can considerably change the temperature regime around the borehole. The temperature plumes become longer as the buried depth increases, which means a longer buried depth yield a smaller temperature variation at any distance from the line source. This is because the heat exchange between the ground surface and BHEs is diminished by the thermal resistance of the ground layer above the boreholes. Therefore, neglecting buried depth could result in an over-prediction of the BHE performance in the design [45].

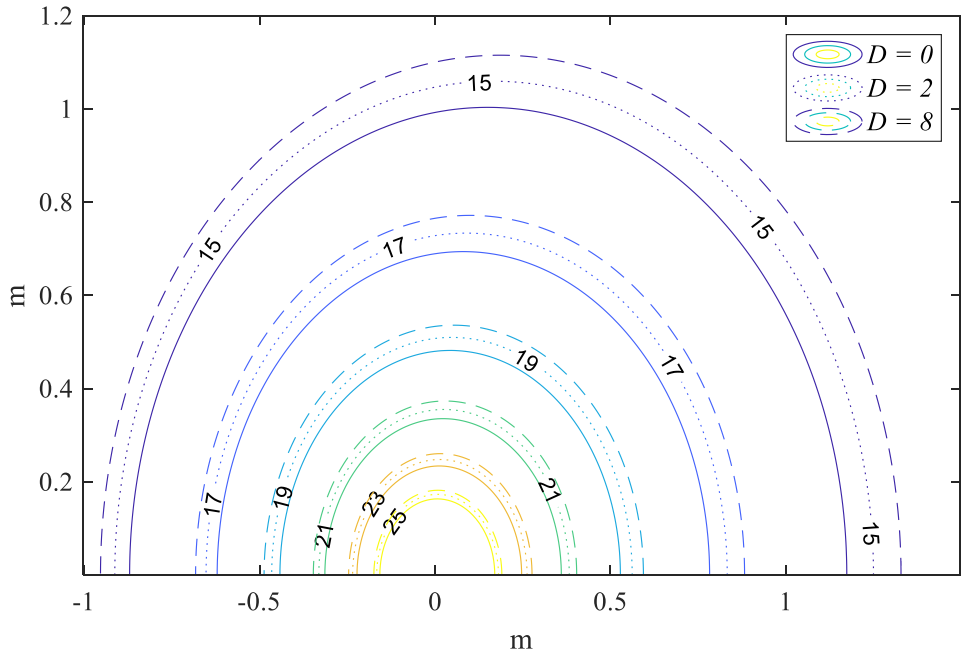

Figure C1. Isotherms of the average temperature variation over the borehole length (H = 70 m) for Pe = 7.5 and various buried depths after 30-year operation.